Master Thesis

Platform development for adaptative auricular vagus nerve stimulation based on cardiac activity

Arnaud Nativel

Mat.Nr.: 11832433

under the supervision of

Univ.-Ass. DI Babak Dabiri Razlighi

Univ.Prof. Dipl.-Ing. Dr. techn. Eugenijus Kaniusas

Research Group Biomedical Sensing

Institute of Electrodynamics, Microwave and Circuit Engineering

Vienna, February 2021

Acknowledgements

I would like to especially thank my thesis adviser Eugenijus Kaniusas for his guidance, help and constant support during the whole research work.

I also own a special thanks to Babak Dabiri who supports me all along my work, introducing me to the research work and providing me with precious advices in numerous domains.

Appreciation is also extended to Klaus Zeiner and all the members of the Research unit of biomedical electronics who welcomed me and provided me all the necessary equipment for this work.

Finally, I also want to thank all my friends and study colleagues for the great time, despite of the special sanitary situation.

Table of Contents

Abstract

Vagal nerve stimulation is a medical act which has been studied since the 2nd half of the 20th century, as a cure for various diseases like epilepsy, though invasive stimulation. Currently, a new site of stimulation though the auricular branch of the nerve offers new perspectives for various positive effects on the patient through non invasive stimulation. In that optic, we designed a software on Matlab associated with a Biopac station, to detect in real time diverse biosignal characteristic from the cardiovascular system, like ECG, PPG, or respiration, and to perform with a microcontroller an adaptative stimulation though a triphasic signal at simultaneously 3 different places of the ear. The aim is to align stimulation events with the temporal activity of the cardiovascular and respiratory system and thus to synchronize artificial stimulus with the intrinsic physiological activity for therapy individualization. The specificity of this platform is the ability to provide a robust detection algorithm of the cardiovascular events, with over 90% detection rate of the R peaks in a noisefree ECG signal with a delay less than 100 ms, to perform the stimulation at a specific time point of the cardiovascular system in real time. The accuracy of the stimulation was tested in open loop with no direct stimulation of the patient and gave satisfying results in term of timing of the stimulation. In the future, it must be tested on real patient to see what kind of impact it will have on the stimulation parameters and on the resulting cardiovascular function in general. The goal would then to integrate this process in an embedded device as a medical cure for various chronic diseases.

Kurzfassung

Die Stimulation des Vagusnervs ist eine medizinische Maßnahme, die seit der zweiten Hälfte des 20. Jahrhunderts als Heilmittel für verschiedene Krankheiten wie Epilepsie durch invasive Stimulation untersucht wurde. Derzeit bietet ein neuer Ort der Stimulation durch den aurikulären Zweig des Nervs neue Perspektiven für verschiedene positive Effekte auf den Patienten durch nicht invasive Stimulation. In dieser Optik haben wir eine Software auf Matlab in Verbindung mit einer Biopac-Station entwickelt, um in Echtzeit verschiedene charakteristische Biosignale aus dem kardiovaskulären System, wie EKG, PPG oder Atmung, zu erkennen und mit einem Mikrocontroller eine adaptive Stimulation durch ein dreiphasiges Signal an gleichzeitig 3 verschiedenen Stellen des Ohres durchzuführen. Ziel ist es, die Stimulationsereignisse auf die zeitliche Aktivität des kardiovaskulären und respiratorischen Systems abzustimmen und somit den künstlichen Stimulus mit der intrinsischen physiologischen Aktivität zur Therapieindividualisierung zu synchronisieren. Die Besonderheit dieser Plattform ist die Fähigkeit, einen robusten Erkennungsalgorithmus der kardiovaskulären Ereignisse bereitzustellen, um die Stimulation zu einem bestimmten Zeitpunkt des kardiovaskulären Systems in Echtzeit durchzuführen, mit über 90% Erkennungsrate der R-Peaks in einem rauschfreien EKG-Signal mit einer Verzögerung von weniger als 100 ms. Die Genauigkeit der Stimulation wurde im offenen Kreislauf ohne direkte Stimulation des Patienten getestet und lieferte zufriedenstellende Ergebnisse in Bezug auf den Zeitpunkt der Stimulation. In Zukunft muss das Verfahren an realen Patienten getestet werden, um zu sehen, welche Auswirkungen es auf die Stimulationsparameter und auf die resultierende kardiovaskuläre Funktion im Allgemeinen haben wird. Das Ziel wäre dann, diesen Prozess in ein eingebettetes Gerät als medizinisches Heilmittel für verschiedene chronische Krankheiten zu integrieren.

List of Abbreviations and Symbols

VNS .... Vagal nerve stimulation

CVS .... Cardiovascular system

tVNS ...transcutaneous Vagal nerve stimulation

aVNS .... auricular Vagal nerve stimulation

AP ....Action Potential

ABVN.......Auricular branch of the vagal nerve

NTS .... Nucleus of tractus solitarius

CVLM .... Caudal ventrolateral medulla

RVLM .... Rostral ventrolateral medulla

ECG .... Electrocardiogram

PPG................................. Photoplethysmogram

FIR...............................Finite impulse response

GUI............................ Graphical user interface

DMA.............................. Direct memory access

DAC ....Digital analog converter

HRV .... Hearth rate variability

S_C ....PPG signal

S_E .... ECG signal

S_R ....Respiration signal

S_T .... Stimulation signal

1 Introduction

Vagal nerve stimulation is a new medical act that has been understudied for some years now and could provide solutions for numerous problems like hypertension or depression. In this work, we interest ourselves in a specific vagal nerve stimulation: the auricular vagal nerve stimulation and the impact that it may have on the cardiovascular system and, more specifically, on the heart variability.

From a physiological point of view, some changes of the cardiovascular system are mediated by a regulatory pathway of the body nervous system called the baroreflex, which modulates the body's blood pressure with different actions on the heart and the vessels. This pathway acts in a closed loop manner and receives feedback from bioreceptors situated in the body, like the baroreceptors which monitor the blood pressure at specific position of the cardiovascular cycle.

VNS could be a way to activate or monitor the activity of this pathway in case of malfunctioning. It could provide a tool to heal chronical diseases that become preponderant today. The development of embedded devices that would be easy to use for the patient and would not be too unpleasant to wear in everyday life is also an essential step in its democratisation.

Thus, this study aims to provide a first step toward more personalized VNS by designing, implementing and testing an adaptative stimulation platform based on individual biosignals, in particular of a cardiac and respiratory origin.

Another following of this study is the possibility of incorporating the VNS into the cardiovascular system's mathematical model. Such in silico model could help us better understand the functioning of the human body and the cardiovascular cycle; it could also be the first step into personalized medicine to find the best cure and cure parameters for each patient.

1.1 Vagal nerve stimulation and relationship with the cardiovascular system

1.1.1 Vagal nerve stimulation

Since the beginning of the 20th century, the human body's electrical stimulations for therapeutic cures have drawn more and more attention. One of those applications is the stimulation of the vagal nerve.

Physiology of the vagal nerve

The vagal nerve, also known as the 10th cranial nerve, is an important nerve of the central nervous system, with a majority of afferent nerves (80%) but with a few efferent nerves, and which plays a significant role in the autonomic nervous system, especially for the parasympathetic branch. It goes from the brain stem to the colon through the neck, the chest, and the abdomen, and it innervates numerous organs of the human body, like the lung, the heart, and organs of the digestive tract. Its role is to transport sensory information on the physiological state of different organs of the body to the brain [1].

Beginning of the VNS

The invasive electrical stimulation of the carotid branch of the vagal nerve has now been used for therapeutic purposes for 30 years and was proven very useful to tackle the problem of epilepsy, that would resist common treatment, through its afferent connection to different parts of the brain as shown in the study of P.Rutecki[1]. Since its validation by the FDA in the USA, many studies were conducted about it and showed its positive impact with a low number of side effects, like sums up the review by J.E Conor Jr et al. [2]. Other studies showed that it could be used for many other applications, like depression [3].

Potential for stimulation of the auricular branch of the vagus nerve

Recently, the auricular branch of the vagus nerve gained a high interest in the VNS field. It has an easy access and has afferent pathways in the brainstem, having a wide range of potential effects, as described in a review by E. Kaniusas et al. [4]:

- **Strokes** where studies in rat showed an improved recovery of the brain tissue after a stroke when paired with the stimulation of the vagal nerve [5].
- **Reduction of chronic inflammatory conditions**, like rheumatoid arthritis, due to the role of the vagus nerve in the regulation of the immune system [6].

Those new applications and others not listed above would go hand in hand with simplifying the electrical stimulation permitted by transcutaneous stimulation. Indeed, transcutaneous stimulation does not require any surgery to place the patient's stimulator and is thus much lighter. Some studies have been conducted regarding its efficiency and side effects: it required much more intensity to stimulate the nerve which may imply other problematics as skin irritation [7].

Glimpse on the cardiovascular effect of tVNS

In the cardiovascular system, the tVNS is received as a promising approach to solve chronic diseases that are more and more preponderant in the population, like hypertension. Recently, the transcutaneous stimulation of the auricular part of the vagal nerve was studied to control the heart rate in a non-invasive way, which could help reduce the effect of some diseases like hypertension [8]. In this paper, they obtained impressive heart rate reduction results when applying stimulations on the ear with a specific set of parameters on test subjects, and they also found an interesting effect of an increase of the heart rate at the end of the stimulation.

Thus, tVNS is still a very young method that has different results depending on numerous factors, and which could also be useful:

- To reduce the arterial mean blood pressure and hypertension. [9]

- To reduce the frequency of arrhythmia. [10]

- To have a positive effect on heart failure by a better control on heart rate variability and the sympathetic/parasympathetic balance. [11]

- To have a positive effect on peripheral blood circulation, that could, for example, improve the healing of diabetic wounds. [12]

1.1.2 Transcutaneous auricular vagal nerve stimulation

Nowadays, many studies and experiments have been conducted concerning the stimulation of the auricular branch of the vagal nerve [13] with varying stimulation parameters to trigger different effects. In the following, we will see the different parameters and their importance.

Position of the electrodes

The electrodes' position is a crucial point to consider, as the nerve fiber's activation depends significantly on their distance from the stimulation point. In most studies, the electrodes are set at various positions depending on the patient and the stimulation device [13]. However, we can note the study by Yakunina et al.[14], who reported the different parts of the brain's activity through fMRI depending on different stimulations cycles and described the cymba combae as the most probable place to get the most of the tVNS, and which could lead to a more systematic positioning on the electrodes.
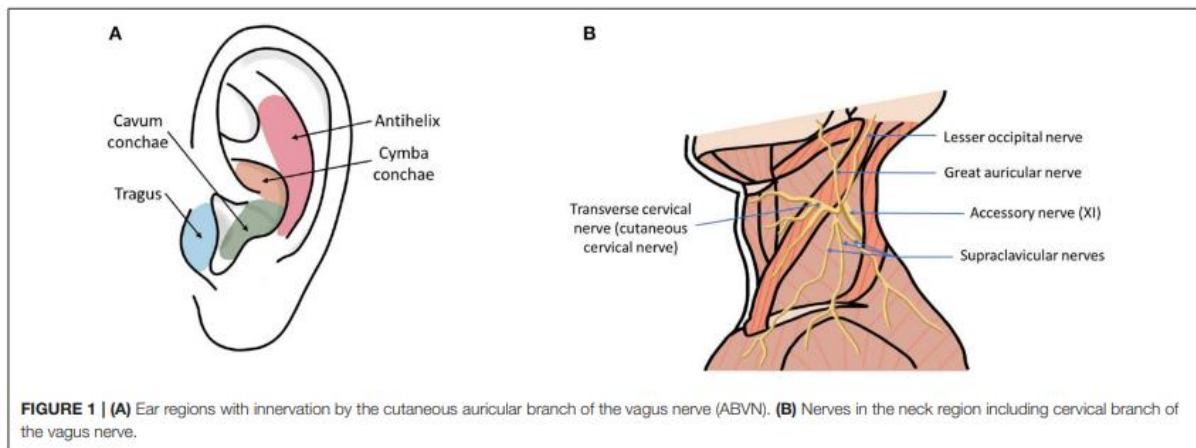

FIGURE 1 | (A) Ear regions with innervation by the cutaneous auricular branch of the vagus nerve (ABVN). (B) Nerves in the neck region including cervical branch of the vagus nerve.

Figure 1-1: Different positions to place the electrodes for VNS [13].

Stimulation intensity

The stimulation intensity and its effects are linked with the electrodes' position. The level of intensity will impact the stimulation in two ways: On the one hand, it will have an impact on the type of nerve fiber stimulated: the bigger the nerve fiber is, and the lower intensity is needed to stimulate; on the other hand, a higher intensity will also permit to stimulate nerve fiber further from the stimulation point, and it will potentially increase the efficiency of the tVNS and stimulate other regions of the brain. In the studies, it is around a few mA, and it is set depending on the patient through their perception of the stimulation. It is often set at the perception threshold, which is the intensity for which the patient will feel a "tickling" or a "prickling" sensation in the region around the stimulation site. The stimulation range can then go until the limited tolerance of the patient, above which the patient will start to feel pain due to the stimulation [13].

Stimulation frequency and stimulation waveform

Two other important parameters concerning the stimulation signal are the frequency and the waveform. Their precise action on nerve activation is still unknown, but through experiments, it has been witnessed different effects on the brain depending on their value. For the waveform, the simplest one to be used is monophasic rectangular pulses, other studies reported using more complex pulses like biphasic or even triphasic pulses, but it is still unclear if they have better efficiency than the monophasic one. The stimulation frequency bears the same uncertainties that the waveform, and even if most of the studies used frequencies in the range of 20-30 Hz, it has not been physiologically proven that it was the most suitable for the stimulation. However, it was thought to avoid severe collateral effects for the vagal nerve's carotid branch's stimulation [13].

1.1.3 Nerve activation function

Type of nerve fiber

Through the electrical stimulation, we want to activate the nerve fibers which are near the stimulation points. The first point to note is that several nerve fibers do not have the same characteristics and the same role. They can be classified in terms of:

- **Myelinated or non-myelinated**: The myelination corresponds to an isolative coating of the nerve fiber by Schwann cells that will accelerate the action potential transmission.

- **The thickness of the fiber**, which also has an impact on the transmission rate of the AP.

Table 1-1: The different types of nerve fibers [41]

Fiber type	Sensory classification	Function	Diameter (mm)	Conduction (m/s)	Local anesthetic activity	Myelinisation
Aα		Motor	12–20	70–120	+	yes
Aα	type Ia	Proprioception	12–20	70–120	++	yes
Aα	type Ib	Proprioception	12–30	70–120	++	yes
Aβ	type II	Proprioception Touch pressure	5–12	30–70	++	yes
Aδ	type III	Pain Cold temperature Touch	2–5	12–30	+++	yes
Aγ		Motor (muscle spindle)	3–6	15–30	++	yes
B		Preganglionic Autonomic fibers	<3	3–14	++++	some
C dorsal root	type IV	Pain, touch Warm and cold temperature	0.4–1.2	0.5–2	++++	no
C sympathetic		Postganglionic Sympathetic fibers	0.3–1.3	0.7–2.3	++++	no

Those different fibers will react differently to external stimulation, and it has to be considered during the stimulation design. According to Yap et al. [13], the distribution of nerves fiber in the ABVN was still largely uncertain in 2016 but was expected to be mainly composed of sensors A-type fibers like Aβ or Aδ, and of C-type thin unmyelinated fibers.

Neuron activation function

The question of neuron stimulation has been well studied during the 20th century. Hodgkin and Huxley performed the first and notable approach with their patch-clamp technique that helped to understand the ionic currents inside the neuron and their role in creating an action potential. This would help them to develop the first and base of a lot of neuron modelling: the Hodgkin-Huxley equation, that will model the electrical behaviour of the cell membrane voltage V depending on the time [15]:

$$I_{stimulus} = C_m * \frac{dV}{dt} + I_{ion} \qquad (1.1)$$

With:

$I_{stimulus}$, the internal stimulus current in the cell

C_m, the membrane capacitance

I_{ion}, the ionic current across the membrane

The specificity of the HH equation lies in the representation of the ionic currents, I_{ion}, summing up the effects of the different voltage-gated ionic channels for the various ion species, mainly sodium and potassium, as well as the leakage current.

$$\boldsymbol{I}_{\mathbf{ion}} = -\mathbf{g}_{\mathbf{NA}}\boldsymbol{m}^3\boldsymbol{h}(\boldsymbol{V} - \boldsymbol{V}_{\mathbf{NA}}) - \mathbf{g}_{\mathbf{K}}\boldsymbol{n}^4(\boldsymbol{V} - \boldsymbol{V}_{\mathbf{K}}) - \mathbf{g}_{\mathbf{L}}(\boldsymbol{V} - \boldsymbol{V}_{\mathbf{L}}) \qquad (1.2)$$

With:

- g_{NA}, g_K, g_L the maximum conductance for each phenomena
- m, h, n the opening probability of the channels which depend on time.
- V_{NA}, V_K, V_L the voltage derived from the Nernst equation apply to each phenomena separately.

From this equation, progress was made regarding the neuron's modelling through a compartmental approach with more and more complex geometry to replicate the propagation of an action potential with current flowing from one compartment to the others (Fig).
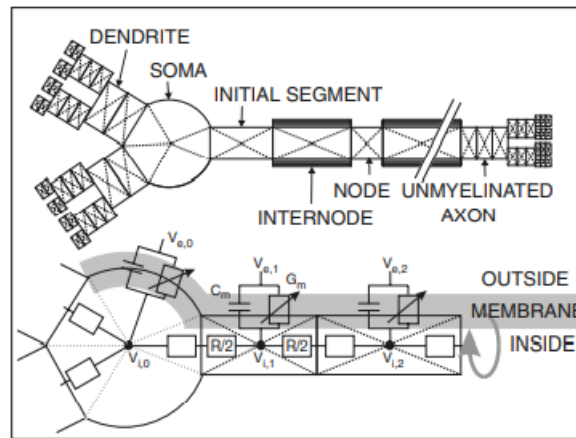
Figure 1-2: Compartment model of a neuron to model the action potential propagation [15].

Such a compartment model linked with the HH equation enables to model the the creation of an action potential from an external stimulus. Indeed, we can observe though the equation that at the beginning of an action potential, the membrane voltage temporal variation is mainly driven by a function of the external potential,

$$\frac{\mathrm{d}V_n}{\mathrm{d}t} = f_n \quad (1.3)$$

With:

$V_n = V_e - V_i - V_{rest}$, the cross membrane voltage difference from the resting potential

which is called the activating function, and has this form if we stay in the compartment model case of the fig:

$$f_n = \left[\frac{V_{e,n-1} - V_{e,n}}{\frac{R_{n-1}}{2} + \frac{R_n}{2}} + \frac{V_{e,n+1} - V_{e,n}}{\frac{R_{n+1}}{2} + \frac{R_n}{2}} \right] / C_n \quad (1.4)$$

With C_n the capacitance of the nth compartment, R_n the resistance of the nth compartment.

With simplication and considering the compartment geometry, it provides one of the interesting points to note is the inverse recruitment curve, which states that the thicker fibers are easier to stimulate [15].

Computational approach

This nerve model can help to model the stimulation in silico to predict what effects it will trigger depending on the parameters. For transcutaneous nerve stimulation, the problem becomes a bit more complicated as the propagation of the electric voltage from the stimulation point has to be considered in 3 dimensions. Fortunately, nowadays, the software can perform numerical computation, thus studied were already conducted to numerically compute the vagal nerve stimulation in response to an electrode stimulation [16]. This kind of study is essential for tVNS and, linked with better anatomical knowledge about the position of the different nerves target for each individual, it may help to place the electrodes more accurately to optimize the effects of the stimulation.

1.1.4 Modelling the cardiovascular system regulation through the baroreflex

Since the 2nd part of the 20th century, many studies have been conducted about the cardiovascular system and its regulatory system, especially baroreflex. To better understand this system and the results of the experiments conducted, mathematical models rapidly became interesting. The cardiovascular system was especially interesting to model as it corresponds to the circulation of the blood in the body through the systemic and the pulmonary circuit and whose circulation is driven by the pressure difference created by the heart. Thus, the equations that drive this system corresponded to the blood circulation's fluid equations and were well known.

Cardiovascular system

The cardiovascular system is the body's organ system whose role is to convey nutrients to the organs of the body and remove their gaseous waste. It is composed of the heart, the arteries, the capillaries, and the veins.

It can be divided into two circuitries, the pulmonary part, which goes through the lung, provides oxygen to the blood, and removes the gaseous waste from the blood. Moreover, the systemic part goes through all the organs of the body for the nutrient exchanges. Both circuitries start and end at the heart site, acting as a pump to move the blood through the vessels.

The heart

As stated before, the heart is the pump of the CVS. It is composed of 4 different chambers: the left atrium, the left ventricle, the right atrium, and the right ventricle, as well as four different passive valves which regulate the exchanges between the chambers with pressure difference. The heart's contraction is due to the regular activation of a group of cells situated at the top of the right atrium called the sinoatrial node, which then propagates an electrical signal through the different muscles of the heart and triggers their successive contraction[17].

Regulation of the CVS by the baroreflex

The baroreflex is a closed-loop mechanism driven by the autonomous nervous system to regulate the blood pressure inside the body. It can be divided into three parts. First, the afferent part transforms the blood pressure at a particular point of the body (the aorta and the carotid) into a train pulse signal to the central nervous system. This part is achieved through the baroreceptors.

The baroreceptors are stretch-sensitive fibers located near the carotid sinus and the aortic arch. The model of those baroreceptors has early been interesting, and the first milestone in their modelling came from the study by Srinivasan et al. [18], which made the first try in linking the carotid baroreceptor pressure to the spike rate of the afferent neuron. They would obtain sigmoid curves relying upon those two parameters. Other studies and experiments followed and helped to understand better the physiological behaviour of the baroreceptors, like the one by Chapleau et al. [19], that presented the results of experiments conducted on dogs to understand the effects of a pulsatile pressure on the baroreceptors. More recently, new techniques are led to a more in-depth knowledge of the baroreceptor at even a smaller level with a study by Soohong et al. [20] that used optogenetic techniques to study the ion channels controlling the baroreceptors' behaviour.

The efferent part of the baroreflex has also been studied a lot. The baroreflex is part of the autonomic nervous system, and its action can be divided into two parts: the sympathetic and the parasympathetic parts. The baroreflex will have different effects on the cardiovascular system: modifying the heart period, the heart contractibility, and the blood vessel resistances. The most studied effect was the heart period modification. This modification is applied by modifying the sinoatrial node, which triggers the heart contraction at regular intervals. During the eighties, several studies by Brown et al. [21], by Jalife et al. |22] helped better understand the heart's pacemaker activity and parasympathetic effect.

The last part of the baroreflex, which links the afferent and efferent pathways, corresponds to the central nervous system. However, due to the extreme complexity of the brainstem, only general studies of the general baroreflex can be conducted to understand its behaviour. In such study, the baroreflex is considered in an open loop, where the aortic pressure is the input, and the frequency of the sympathetic and parasympathetic nerves are the output. Therefore, the baroreflex is then represented as the product of transfer functions. One example is the study by Kawada et al. [23], which used experimental data on the rabbit to adjust the baroreflex characteristics in the dynamic case.

With such approximations of the different parts of the system, it has become possible to model the whole system with both cardiovascular dynamic and the baroreflex creating a closed-loop system. One of the first models to link the cardiovascular system and the baroreflex was released by Ursino [24]. It was the first model to give a clear mathematical framework to the relation between the two systems and better understand it. It was followed by other models that would consider more elements like the chemoreceptors in the model by Ursino et al. [25]. Those models were then reused in other research to investigate the effects of different phenomena on the link between the baroreflex and the cardiovascular system, the baroreflex sensitivity, as in the study by Berteotti et al. [26], which focused on the effect of sleep on baroreflex. In this domain, Silvani et al. [27] study, which overlooked the effect of the central autonomic control on the cardiovascular system and its interaction with the baroreflex, is also interesting.

Modelling of the tVNS

A future evolution to those cardiovascular models could lie in the integration of model of the therapeutic interventions. A particular difficulty in modelling the auricular branch's VNS stimulation is the knowledge of the part of the model on which it would apply [28]. In a recent paper about the computation of cervical vagal stimulation, they model the stimulation by direct addition to the heart period using a coupled transfer function to transform the electrical stimulation into a temporal delay. However, other studies also showed that those stimulations might have an indirect impact by exciting several brain parts like the tractus solitarius or the locus coeruleus. The study [14] using fMRI highlighted that tVNS in the auricular part would have an excitatory effect inside the nucleus of tractus solitarius (NTS).

To model such an indirect interaction, it may then be interesting to have a more detailed simulation of the baroreflex at the brainstem level.

1.1.5 The baroreflex in the central nervous system

Nucleus of tractus solitarius

In the following, I will summarize the knowledge about the baroreflex's physiological part in the brainstem. The baroreceptors synapses are connected to a part of the brain called the nucleus of the tractus solitarius [29]. The baroreceptors will have an excitatory effect on the neurons of the NTS. The NTS is then connected to different brainstem parts: the ventrolateral medulla corresponding to the sympathetic pathway and the nucleus ambiguous for the parasympathetic pathway.
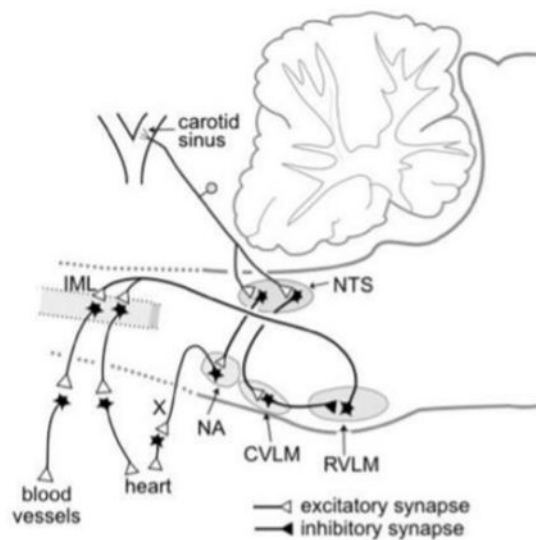
Figure 1-3: Schematic diagram of the baroreflex pathway in the CNS, CVLM caudal ventrolateral medulla, IML intermediolateral cell column, NA nucleus ambiguous, NTS nucleus tractus solitaries, RVLM rostral ventrolateral medulla [40].

A recent study [30] gives a more detailed view of the functioning of the NTS. They used Calcium imaging to understand the critical role that astrocytes have in the NTS, especially for the baroreflex. They proposed a model explaining how the NTS neurons process the incoming

signal from the receptors to create an output signal going to the other pathways: sympathetic and parasympathetic.
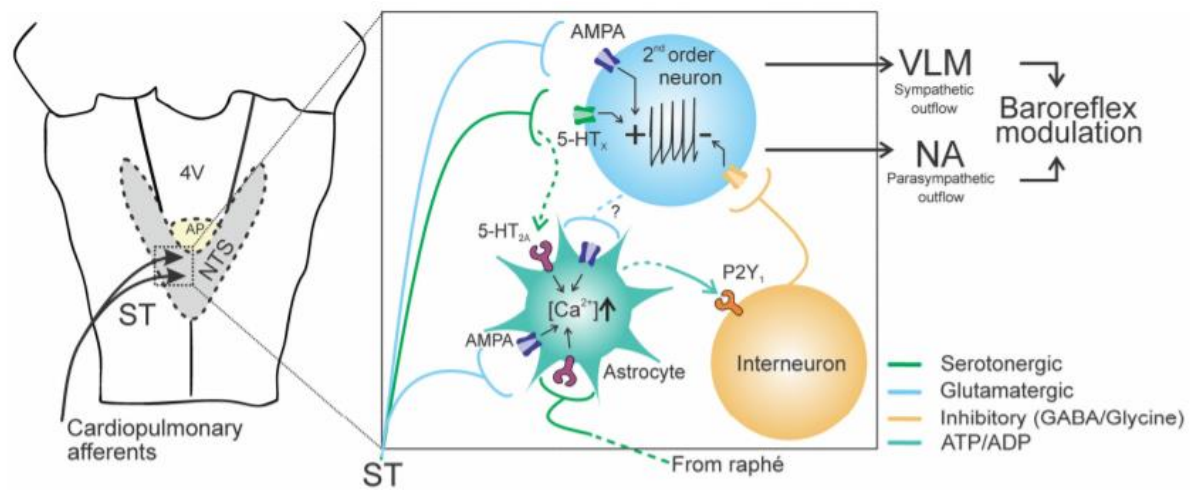
Figure 1-4: Model of the neuron's interaction inside the NTS [30].

The sympathetic pathway
The central nervous system's part of the sympathetic pathway has also been studied a lot. The processing is done in the ventrolateral medulla in the brainstem. First, the signal from the NTS goes to a group of neurones in the caudal ventrolateral medulla (CVLM) in an excitatory action and this excitatory action then create an inhibitory action in the rostral ventrolateral medulla (RVLM), which then send the signal to the different parts of the cardiovascular system. One of the most studied group of neurones are the sympathetic preganglionic neurones that will process the inhibitory signal from the RVLM but also from other parts of the brain and which even have a pacemaker-like activity [31].

The parasympathetic pathway
The parasympathetic part is achieved in another part of the brain called nucleus ambiguous (NA). This part has also been studied from a physiological point of view; it receives inputs from different parts of the brain but especially from the NTS for the baroreflex. One distinct group of neurones in the NA are the vagal preganglionic neurones that are efferent neurons that will send the signal to the heart [32]. This parasympathetic neuron activity will increase with the baroreceptor activity and decrease the heart rate through interaction with the sinoatrial node.

About a more accurate model of the baroreflex
All those papers can give a brief overview of the baroreflex's physiological constitution; even they are only of small parts of the whole cardiac autonomic system that helps to control the pulmonary-cardiovascular system. In the actual model linking the cardiovascular system with the baroreflex, the baroreflex is often represented as a transfer function that does not consider any physiological aspects of the baroreflex. We could then wonder if it would not be possible to use our knowledge of the constitution of baroreflex to create a more interesting mathematical baroreflex model, which would also make possible the addition of other elements of the central nervous system that helps to control the cardiovascular system, for example, the reset of the baroreflex [33]. The question would be how to model it in itself and which characteristic

variables of a neurone could be used. Some papers [34][35] could give a glimpse of the response. It tends to model the interaction between a group of neurones and gives differential equations linking the postsynaptic potential and the corresponding neuron's activity. The most challenging part comes from validating such a model; indeed, it seems complicated to access in vivo experiments giving such precise information. A partial solution would be to consider the whole system's response to constant input, see the steady-state response, and tune the model's constants to find the characteristic curves, often sigmoidal, of the existing models, the baroreflex.

1.2   Statement of the hypothesis/research question:

This work aims to prepare a platform that provides a controlled loop to stimulate the auricular branch of the vagal nerve at specific cardiac and respiratory cycle moments. Bio-signals like ECG, pulse Photoplethysmogram, or respiration as feedback are sensed to target a specific physiological heart event to fire the stimulation. This platform considers the cardiac and respiratory events and the stimulation parameters like amplitude, burst duration, and delay to study the resulting outcome due to the stimulation itself. Since the CNS regulates the cardiovascular system by monitoring the pressure level as input via baroreceptors, this platform will provide a conditional stimulation for the higher-pressure level in the systolic phase with more sensitive baroreceptors rather than the diastolic pressure to investigate whether the stimulation is more effective or not. Nevertheless, other events of the cardiac cycles can be investigated throughout the stimulation. Adapting to the heart rate variability and real-time bio-signal acquiring, and precision of stimulation firing is the aim of this study.

2 Methodology

2.1 General idea

The main aim of this platform is to follow the temporal development of the cardiovascular cycle in real time to be able to stimulate it at chosen timing. This monitoring uses biosignal, which is the description of a physiological phenomenon, here the heart cycle. This report will then follow the process's temporal behavior from the biosignal acquisition and its processing to the creation of the stimulation order in adequation to the heart cycle history provided by the biosignals.

For this work, we have been using three different hardware devices that perform specific tasks.

First, we use the MP34 station from the brand BIOPAC (BIOPAC system, inc., Goleta, California, USA) with the associated sensors, which enables converting and recording different types of biosignals as electrical signals in real-time. The MP34 could receive four different biosignals simultaneously but could output only one (the 3rd channel) as an analog signal. This channel three was connected to an A/D converter from Texas NI, which would then output to a computer port.

The next step was done through a computer. This computer would perform the postprocessing of the used biosignal and create the stimulation command signal. The postprocessing step is done through the software Matlab (The MathWorks, Inc, Natick, Massachusetts, USA) associated with Simulink. Matlab is a programming software specialized in numerical computing, the addition of the Simulink module make it more adapted for real-time stimulation and embedded system. Simulink is also well adapted to have a good visual representation in a linear process of data. It uses blocks that perform specific actions, exchanging data between each other through input and output ports.

Through this work, we have been using the Matlab version 2020a. Another advantage of Matlab is that it comes with a certain number of packages for various application domains. In our work, we notably used the data acquisition module to receive data from the I/O converter.

Finally, the last PC is a microcontroller of type STM32 powered by a 3.7 V battery that fires the stimulation via electrodes when it receives the PC's triggering signal via serial connection.

The stimulation signal is just a triphasic signal sent simultaneously at three different external ear parts with a phase shift.
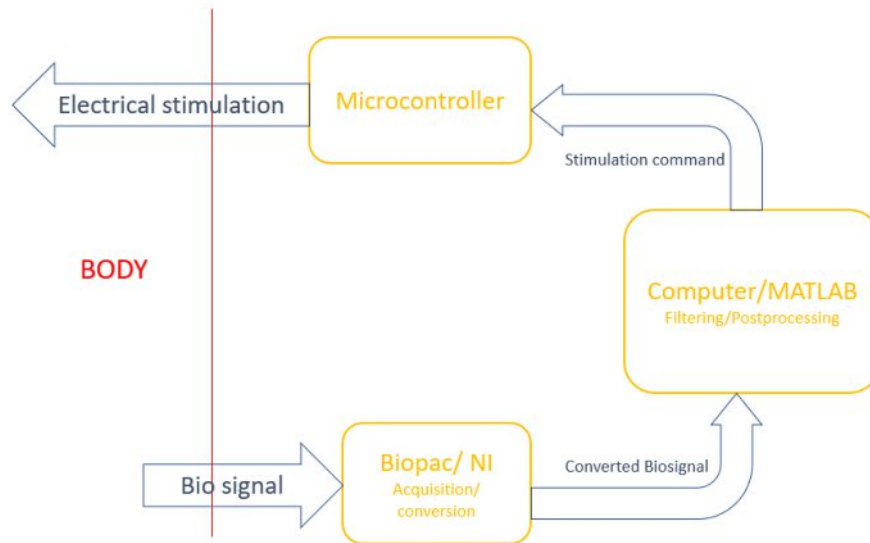
Figure 2-1: Schematic of the whole data circulation of the platform.

2.2 Bio signal acquisition

Type of Bio signal

To follow the cardiovascular system's state and its phase, we are using bio signals related to it. In this study, we are going to use 3 bio signals: the ECG, as S_E in the figures, the PPG, as S_C, and respiration by chest-belt, as S_R.

The ECG and the PPG are related directly to cardiovascular cycles and have the same role in our algorithm. The main notable difference is the time delay between the two signals, as depending on where the PPG sensor is situated, the pressure wave needs some time to travel from the heart to the sensor place.

The chest-belt is a bit different as it mainly records the respiration activity, which has a longer period than the cardiovascular cycle and is composed of two phases: inspiration and expiration. We recorded this signal as the respiration is expected to have some interactions with the baroreflex.

- ECG:

The ECG which stands for Electrocardiogram represents the electrical state of the heart at a certain period. From a physiological point of view, this electrical field is generated by a group of cells situated at the sinoatrial node next to the right atrium of the heart and then propagates along different cells of the heart triggering the contraction of different heart muscles. By recording the potential differences in the body at a minimum of two points of the body we can witness this changing electrical field due to the heart activity [17].

In our study, we have been using a 3-point ECG, according to the Einthoven triangle, see Fig 2-2:
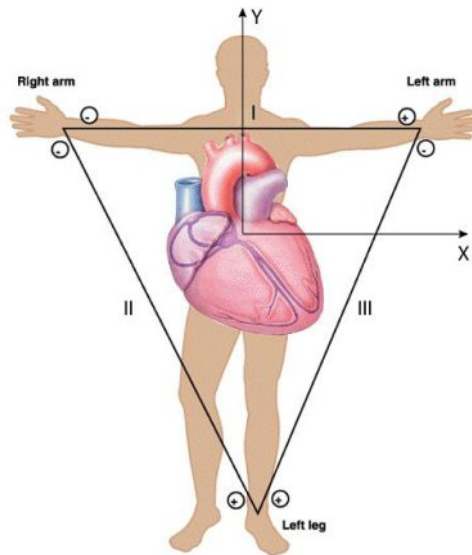
Figure 2-2: Einthoven triangle for ECG [42].

The typical form of an ECG is shown in the following figure 2-3:
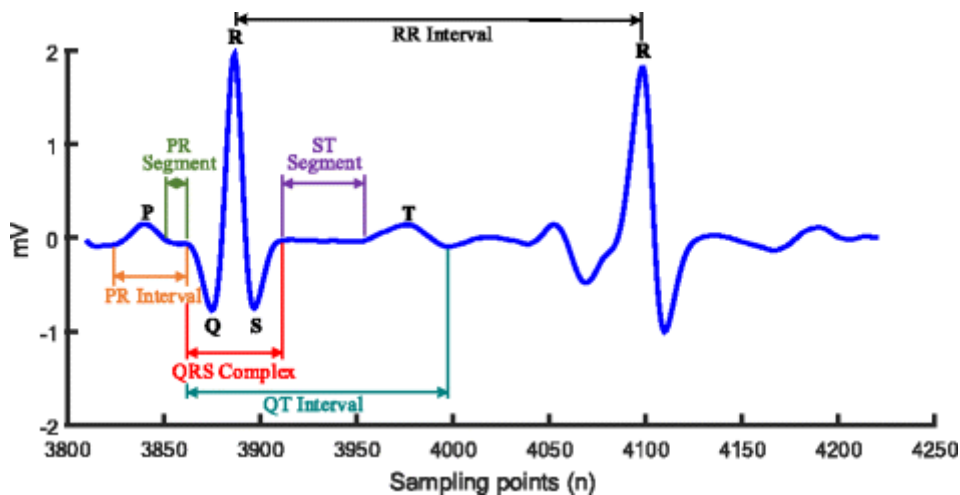
Figure 2-3: Example of an ECG [43].

We can distinguish five typical peaks: The P, Q, R, S, T peaks, each associated with a different heart state. The most used peak of the ECG is the R peak, as the most easily detectable peak, even in a noisy signal. Its narrowness enables a good precision in situating it in the time domain, explaining its predominance for the heart rate calculation; we then speak of R-R interval.

- PPG:

The PPG, or photoplethysmogram, corresponds to blood volume changes in a microvascular bed of tissues. It uses the different light absorption due to changing blood volumes following the heart cycle phase. In our study, we have been using the PPG at the tip of a finger. The general form of a PPG signal is (Fig. 2-4):

14
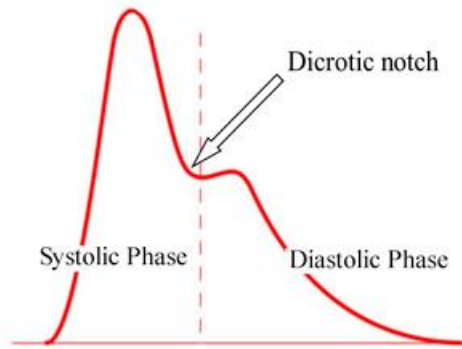
Figure 2-4: PPG pulse wave form [44].

We can recognize two phases: the systole, which corresponds to the increasing part, and the diastole, which is the decreasing part. PPG is a well-studied signal, which gives a lot of information about the cardiovascular system and the state of the blood vessels of a patient. For our study, the most important point is that the PPG isn't directly time synchronized with the heart cycle, as it needs time for the pressure wave to travel along the arteries until the recording point. This delay is however constant from one cycle to the other and can be approximate by knowing the distance between the heart and the recording point [17].

- Respiration:

The last bio signal which we have been using is the chest-belt which measures the chest diameter changes due to the respiration cycle. The typical form of such a record is:
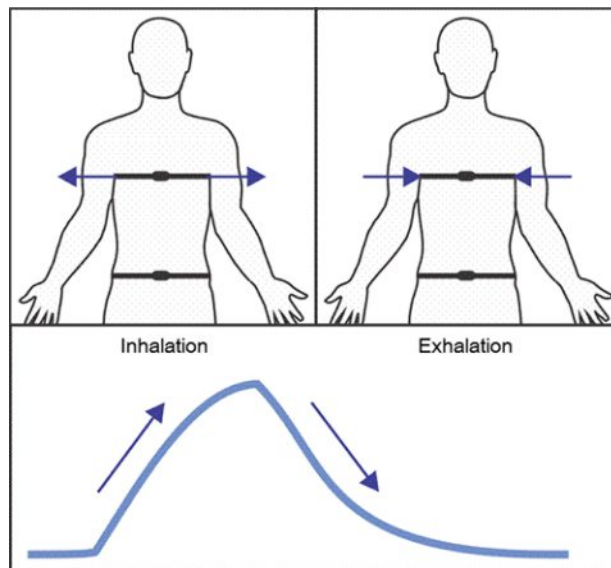
Figure 2-5: Respiration belt and associated biosignal. From the Respiration sensor datasheet by ThoughtTech (ThoughtTech, Montreal, Quebec)

We can distinguish two phases: the inspiration and the expiration. The respiration cycle has a bigger period that the cardiovascular cycle and there are interactions between the 2 cycles at various point of the organism.

Acquisition of the bio signal

To process the signal through the computer, we must convert it from an analog to a digital signal. As we showed in the general schematic of the system, this is done by a hardware I/O converter (National Instruments Corporation, Austin, Texas, USA) with the Data Acquisition (DAQ) module of Matlab , specially designed for this kind of instrumentation. For this conversion, we must set two important parameters:

The conversion frequency: the frequency at which the analog signal will be converted; the highest the frequency, the more noise in the signal, but the more precise it will be. We have decided to use a 500 Hz conversion frequency in our work, so a data point every 2 ms.

The transmission frequency: once a point data is created, it is saved in an internal buffer. The transmission frequency of this buffer into Simulink can be set. The value will depend on the objective and on the characteristic time of the considered biosignal. For the ECG and the PPG, it corresponds to the heart period around 0.8 s. That is why we decided to take the maximum frequency allowed by the Matlab DAQ module, which is 20 Hz. So, we finally sent 25 data points every 50 ms. It is quite different for respiration as respiration is more prolonged, around a few seconds, and that is why we could take a smaller acquisition frequency of 2 Hz.

This acquisition step enables us to have a good visualization of the biosignals in real time (Fig 2-6, 2-7). S_E stands for the ECG outcome and S_C corresponds to the PPG signal.
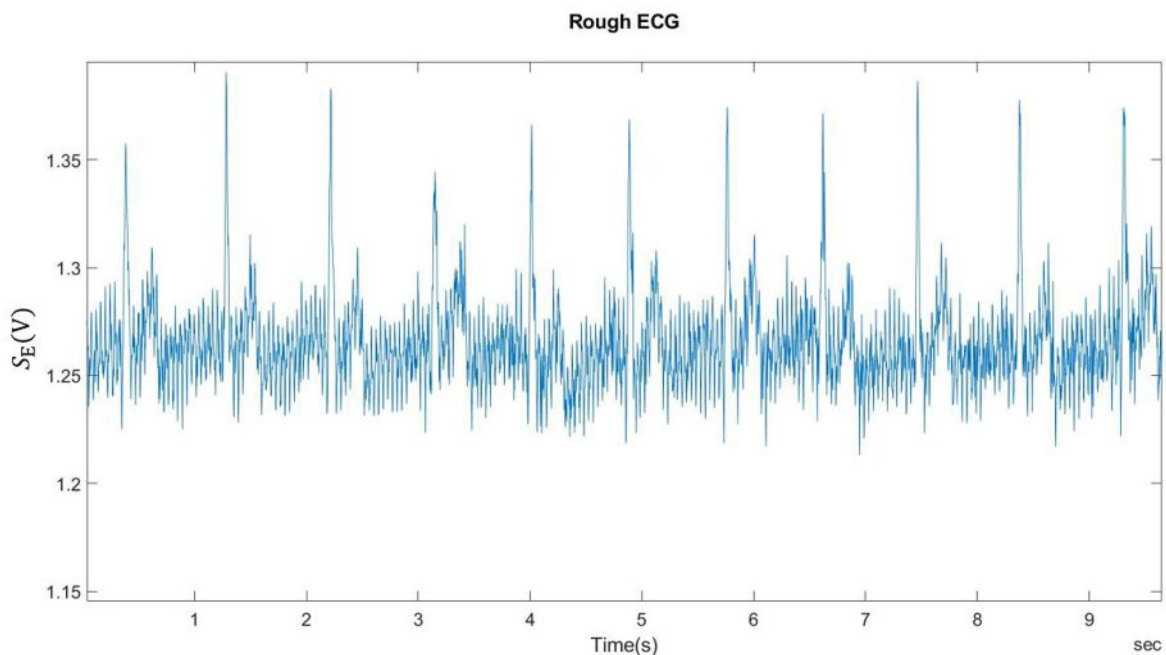
Figure 2-6: ECG signal obtained by the plateform for a 500 Hz acquisition frequency.
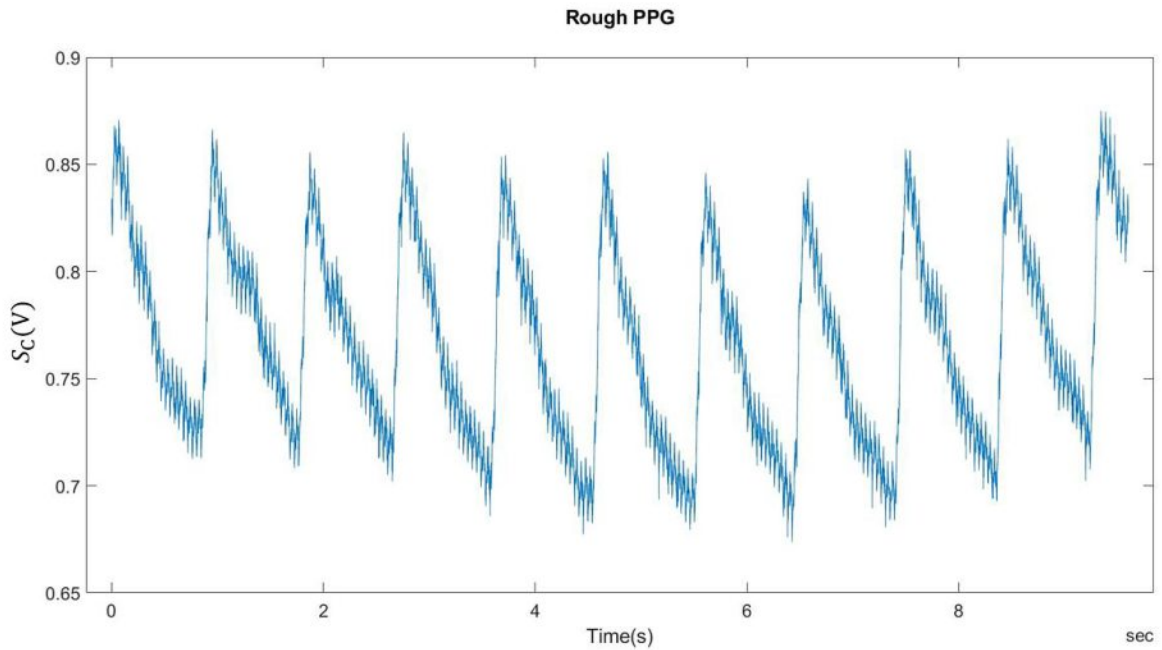
Figure 2-7: PPG signal obtained by the plateform for a 500 Hz acquisition frequency.

Filtration of the bio signal

As the human body is a complex environment with many simultaneous phenomena, the biosignals are often the result of interferences between those different phenomena. That is why a filtration step is necessary to study a system like the cardiovascular one. Another predominant noise that must be eliminated by filtration and often found in such experiments is the noise due to the power supply, often around 50-60 Hz, see Fig. 2-8.
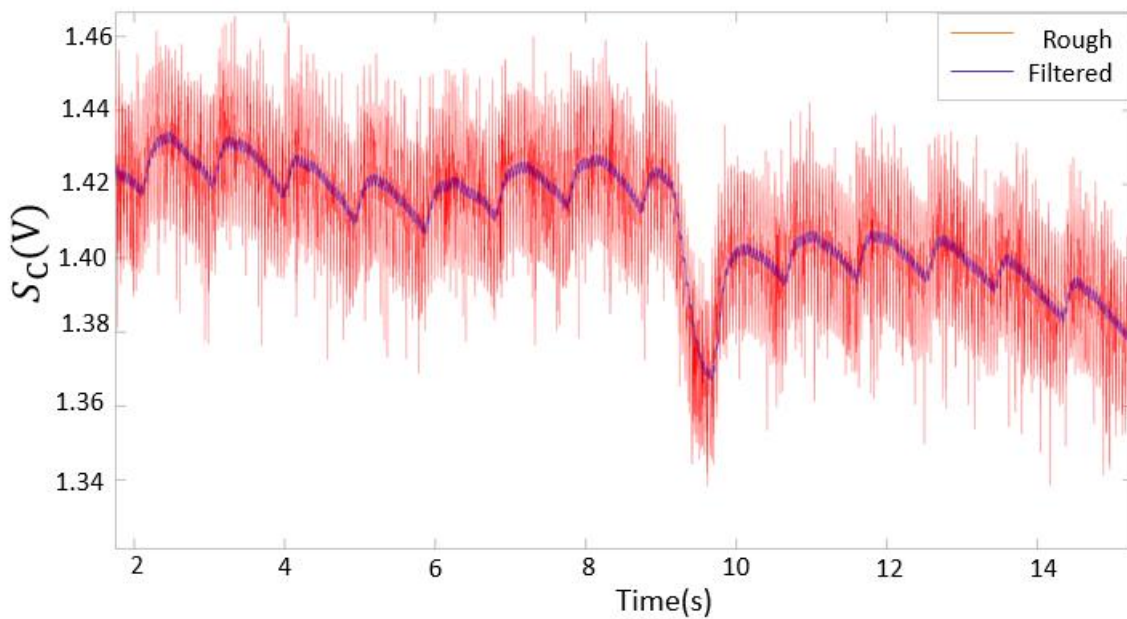
Figure 2-8: Example of a PPG that we recorded with strong noise and movement artefact. The signal was filtered with a low pass filter with a 15 hz cutting frequency.

To process ECG or PPG, the basic idea is to use both lowpass and high pass filtration to eliminate the base drift and the power supply noise, and to keep the interesting frequency between 0.5 Hz and 15Hz.

However, our case is a bit different as we are processing the data in real time, it means that we can only apply FIR filters because we received the data one after the other. We must also take care of the delay that is created by the filters, the bigger the order of the filter is, the later we are in comparison with the real signal. Taking that in consideration, we noticed that the biggest interference to the signal were coming from the power line frequency. And we could get rid of it by using a FIR lowpass filter using the Barlett-Hanning-Windows with a cutting frequency around 15 Hz and with an order of 70 which would represent a 70 ms delay, see Fig 2-9.
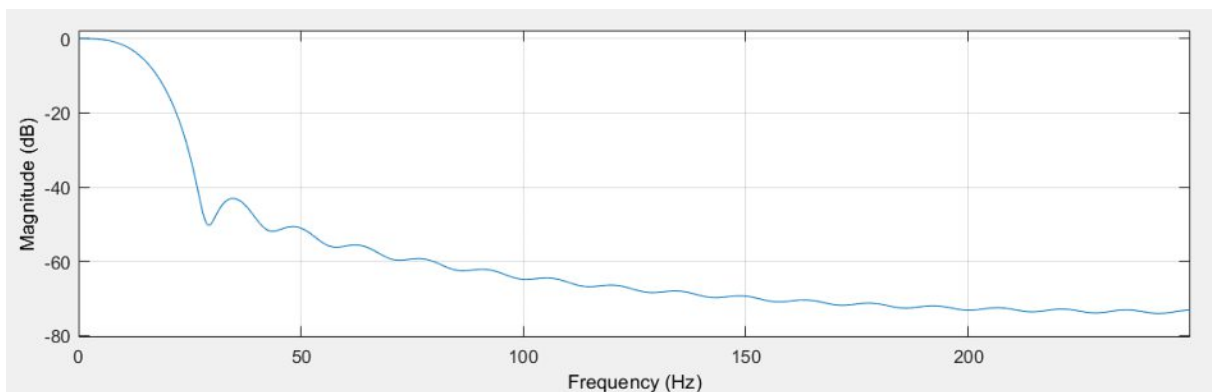
Figure 2-9: Bode diagram of the low pass filter.

The processing of the data is done sequentially in Simulink. We filter the data every 50 ms at the same time as acquiring the 25 new data. However, at each filtering step, we considered the new 25 data samples and the 70 previous ones to fit the filtering order. This is summed up in the schematic here:
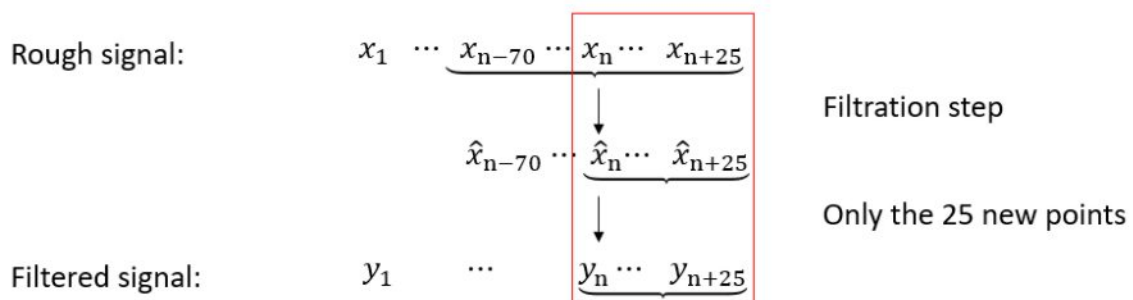
On the contrary, we couldn't use FIR high pass filter as the required order for a good result was far too high due to the narrowness of the cut band 0-0.5 Hz compared to the sampling frequency 500 Hz.

Movement artefact:

The second major issue while processing biosignal is called movement artefacts, noise in the signal due to the movement of the recorded patients. They are harder to filter as their fundamental frequency is often situated in the same range as the frequency domain that we are interested in, and thus it will require a complicated filter to get rid of them. Nowadays, some methods achieve to tackle those issues. One of the most promising approaches that we tried to adapt to our problem was the weighted Fourier linear combiner, a kind of adaptive filter based on least mean square calculation.

The main medical application is for robotic arms in surgery to detect and remove the surgeon's trembling over operation [36]. The idea is to approach the input signal with a combination of sinusoidal function with adapting coefficients calculated at every step of the process from the error between the approximate solution and the real signal. We tried to combine several of such filters with varying converging coefficients, and even if we had some results, it was not robust enough for simple movement artefacts. Some other propositions are derived from adaptive filtering in the literature, for example, adaptive notch filtering (ACF) [37]. However, in the proposed algorithm, they would have a delay of few seconds, which is not suitable for our case, where we consider the real-time to be our prior consideration.

 A solution to compensate for the movement artefact would be based on adaptive noise cancellation techniques that would use other sensors like accelerometers to detect the movement directly and help correct the signal.

Finally, as we wanted to keep a simple solution, we decided not to remove the movement artefact but to detect it in our signal and not to launch a stimulation if some were detected. We based our detection algorithm on a paper [38]. This algorithm is based on a cross-correlation coefficient analysis between a detected pulse from the incoming signal and a standard pulse template. It is based on a simple comparison. If this cross-correlation coefficient is above a certain threshold, it means that the signal is still readable and there is no movement artefact. On the other hand, if the coefficient is under the threshold, there is some movement artefact, and the stimulation is cancelled until we find the next correct pulse from the input signal. We implemented a version of this algorithm in Simulink; however, it poses a certain problem regarding the calculation constraint inside Simulink, so we had to avoid it and assume that there would be no movement for our manipulation's artefacts.

Concerning the MA detection algorithm, we would explain it more in detail in the appendix.

2.3   Creation of the stimulation order

General consideration

Once we acquired the signal, a decision process must decide when to start the stimulation. This stimulation point is a predicted moment from the last heart cycle. A reference point that enables the stimulation to adjust the start of stimulation with specific delay corresponds to that. Of course, the signal acquiring process poses some delay to the system, which should be considered. Knowing this reference point and adjusting the magnitude or the burst duration of the stimulation provides a flexible stimulation setup based on biofeedback.

Direct stimulation

For the respiration cycle, it will be well adapted; indeed, there are two major phases: inspiration and expiration, and by just studying the slope of the corresponding bio signal: the chest diameter, we can know in which phase we are, and decide to stimulate or not. For each incoming segment of 250 data points, we calculate the segment's slope using the polyfit function of Simulink, and we compare it to a threshold: positive for the inspiration and negative for the expiration, see Fig. 2-10. In the bottom plot of the figure, the stimulation signal, as ST, represents the state of the stimulation: 0 for no stimulation and 1 for ongoing stimulation.
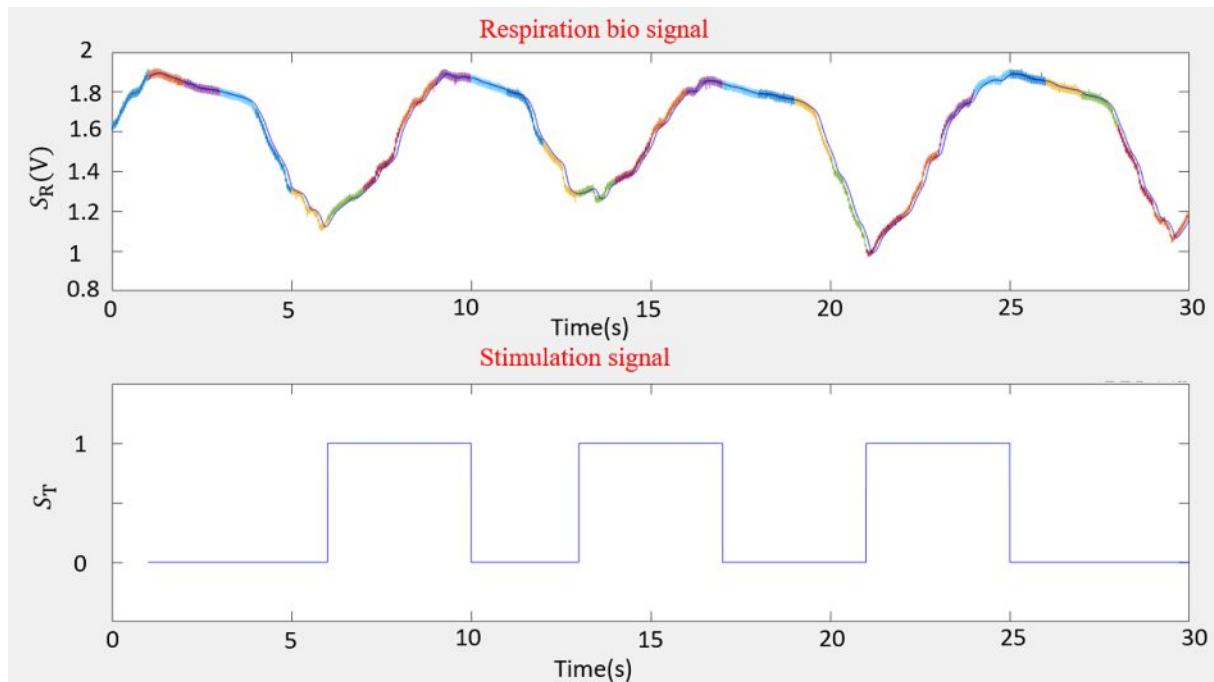
Figure 2-10: Screenshot of the processing result for respiration with the respiration bio signal at the top and the binary stimulation command at the bottom. Top: The different colors represent the 25 sample data buffer received by the Matlab software every 50 ms.

Here we can see the stimulation activation or not, depending on the respiration slope. The top curve shows the respiration signal, where each color segment represents a train of data acquired by the software at the same time.

For the cardiovascular cycle, this is more complicated. The target stimulation interval is the systolic phase, which corresponds to the increasing part for PPG and the QRS complex for ECG. However, this phase only lasts for 250-300 ms, and if we consider the latency due to the communication between the different hardware parts of the plateform, which is around 100 ms (see part 5.3) and the delay in the software due to the data buffer and the filtering process , also around 100 ms, the stimulation will likely miss the systolic phase.

Predicting stimulation

For ECG and PPG, the solution is then in predicting the upcoming systolic phase to fire the stimulation out of last detected systolic phase. Here come two major issues, first we should determine which part of the bio signal to identify and then calculate an approximate delay between the detected phase and the actual target point for the stimulation. Here is a schematic for an ECG (Fig. 2-10). Regarding the plotted ECG biosignal, it corresponds to a template extracted from a 120s ECG signal, whose each heart cycle has been separated using the Q-

peaks. Each separated cycle follows a postprocessing step; being normalized between 0 and 1 both in time and in amplitude before a resampling into 256 data points. We then perform a principal component analysis to the obtained data to obtain the main component that becomes our template.
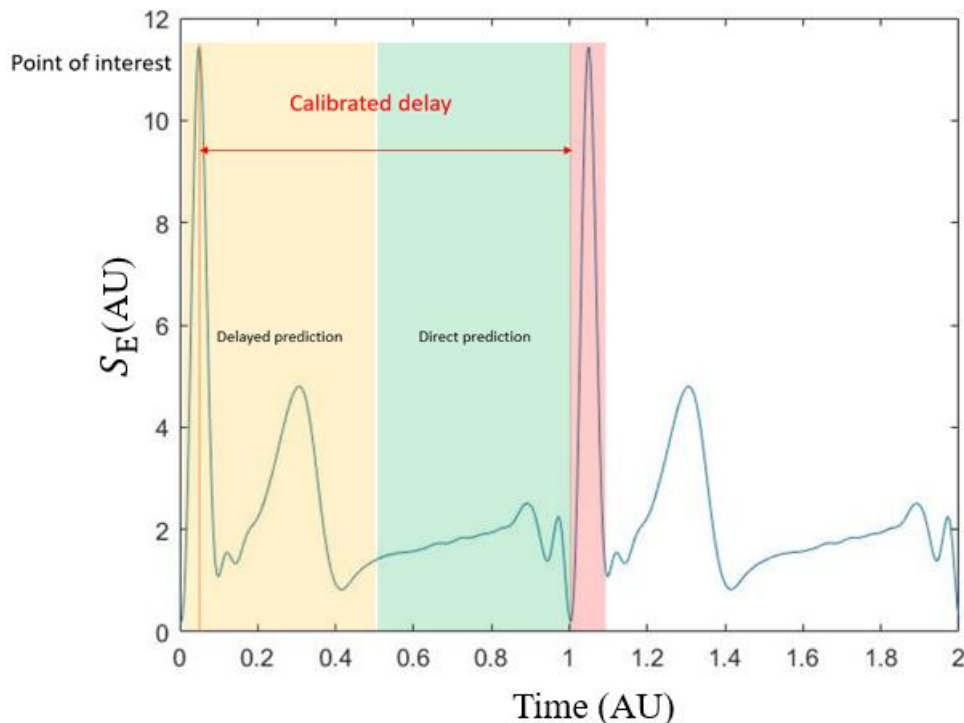
Figure 2-11: Schematic of the stimulation process for ECG. The graph shows consecutive two heart cycles whose period have been normalized to one. The red part shows the optimal stimulation target.

Fig. 2-11 shows two possibilities; the first one is called an immediate prediction (2-10 colored); we try to detect the phase just before the systolic phase to have enough delay to fire the stimulation at the time of the systole. However, this part of the signal is unstable, and it can be quite hard to detect. This would require too many calculations for a robust algorithm.

The second solution and the one that we implemented is to detect an interesting point of the biosignal, which is easier to assess and calculate statistically for a given patient an approximation delay when the next systolic phase will come. In the next part, we will show it for the two biosignals ECG and PPG.

For ECG, we want to detect the R peak. The R peak detection and even the QRS complex detection are widely studied, even more since the arrival of embedded devices for everyday life monitoring. Thus, it exists several methods to perform the detection, from the simple Pan-Tompkins algorithm with adaptative thresholding [39] to more recent methods using wavelet transform or artificial neural network. The main limitation to those methods is that they need a high pass filtering to remove the drift, which is too complicated regarding our delay constraint. We also wanted to employ a faster process for our live process without too much computation, and we were limited in our data manipulation by using Simulink; that is why we only used a slope threshold-based detection algorithm.

For each incoming 25 data point, we calculate the slope after low-pass filtering, and by comparing it with a positive threshold, we want to know if we are in the Q-R phase of the QRS complex. Then, once such a slope is detected, we are looking for the next local maximum of the signal, and we label it as the R peak. Considering the slope enables us to completely get rid of the base drift impact on our process.
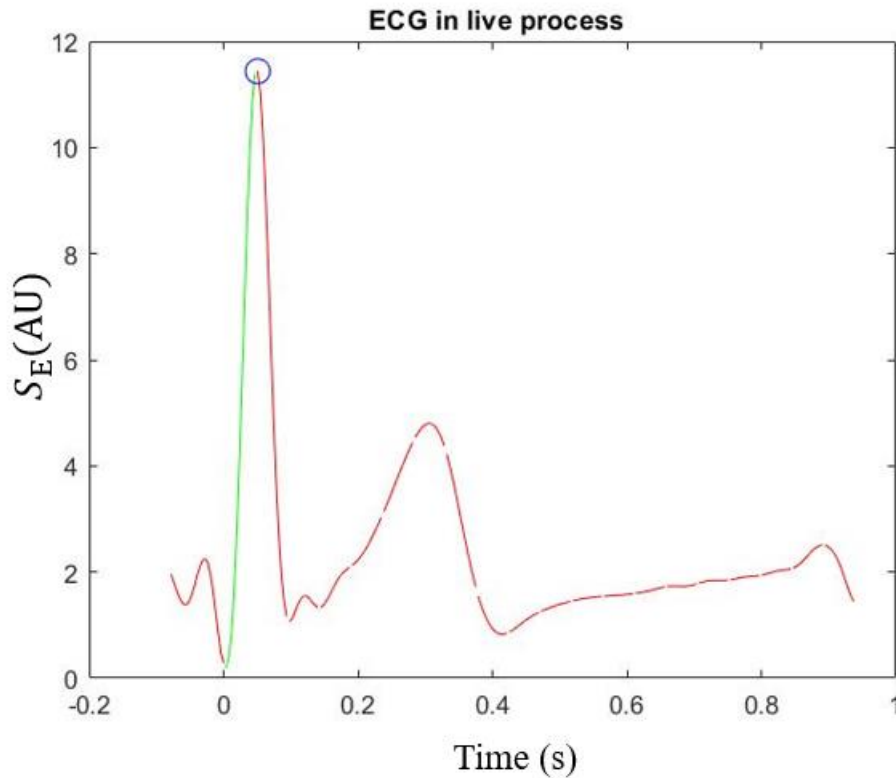
Figure 2-12: Example of an ECG incoming signal (same template than Fig 2-10) cut into continuous segments of 25 data samples, that are received by the Matlab software at the same time. The color correspond to the outcome of the slope detection process, red for under the threshold and green for above.

In figure 2-12, we see the optimal detection situation, where the incoming data are situated precisely on the QRS segment and gives the highest slope.

For PPG, our point of interest corresponds to the top of the systolic phase. However, as we only consider the specific part of the signal, it is hard to find a local maximal. That is why we decided to first detect the slope of the systolic phase; as for the ECG: we compare the slope for each incoming input to a certain threshold, and once this threshold is overcome, we look for the next local maximum. This live decision process is showed in Fig. 2-13. The used PPG bio signal template was obtained with a process similar to the one used to get the ECG template.
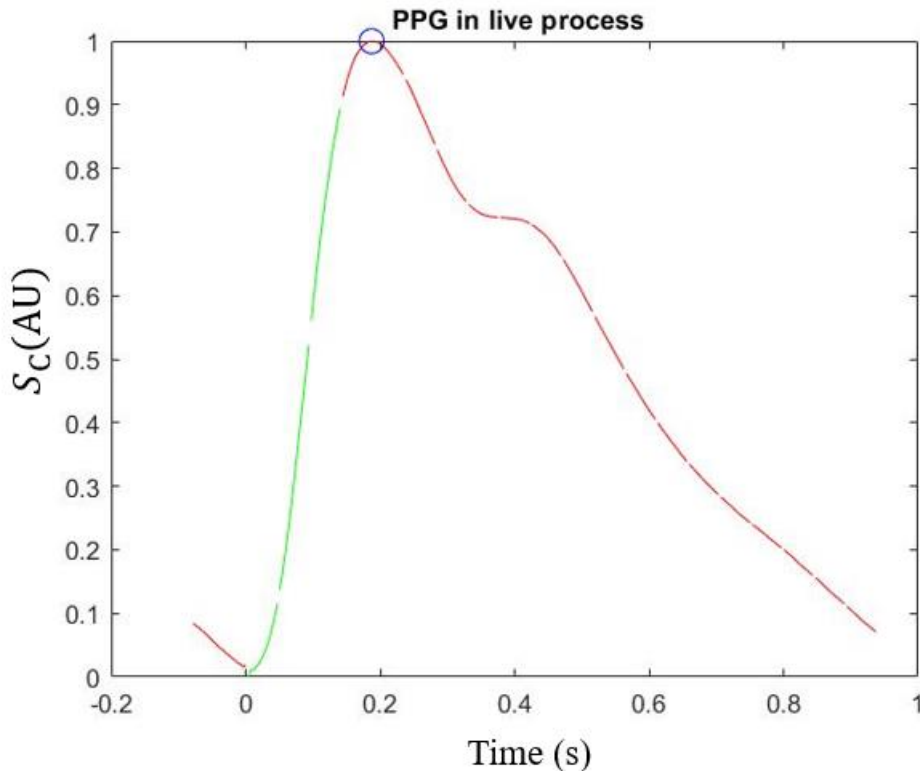
Figure 2-13: Example of an acquired PPG signal cut into 25 data sample and highlight with the results of the slope comparison. Red segments correspond to the segments below the threshold and green segment to the ones above.

When an interesting point of the bio signal, either ECG or PPG, is detected, we then wait a certain delay that has been calibrated before firing the stimulation, in that way we expect to have the stimulation during the targeted period of the next cardiovascular cycle.

2.4 Calibration

With such detection and stimulation, a calibration phase becomes necessary to assess the appropriate values for the different parameters, which will depend on the patient's state at a given moment: the threshold for ECG and PPG, and the delay between the detected event and the target stimulation period.

This calibration phase is done before the beginning of a stimulation session. We record the patient's biosignal, and we filter it using the same filter as for the live process. For ECG, we find the R peaks using findpeaks function of MATLAB, and we find the Q and S peaks by looking for local minimum on neighboring intervals of the R peak.

For PPG, we look for systolic peak using the findpeaks function of MATLAB with parameters, and we set the diastolic valley as the local minimum of a given period before the systolic peak.

We then have for the recorded bio signal a given number of pulses whose interested points are known, and we can then calculate for each pulse the value of the slope and the delay between

two pulses, like in the schematic. We take the 25th quantile value of the data for the given pulses for the threshold, and we downscale it by a specific factor.

We decided to take the 25th quantile because we are selecting all the segments whose slopes are above the threshold value in our processing. By reducing the threshold compared to the median value, we are increasing the number of detected pulses. It would be possible to decrease the considered quantile; however, we would increase the possibility of false-positive detection in the real-time process or even consider outliers in the calibration phase. To compensate for the theoretical loss of 25% of the data, we also downscale the threshold T by an arbitrary factor α to detect a larger number of pulses (2.1).

$$T = \alpha * Q_{25} \quad with \: \alpha \: \in \:]0; 1[\qquad (2.1)$$

With:

- Q_{25}, the 25th quantile of the slope distribution determined on the calibration data

For the calibration delay, this is a bit different. Indeed, in real-time, the delay between the point of interest, for example, the R peak, and the next systolic beginning, depends on the heart period, and the accuracy of the stimulation will then depend on the heart variability. We chose to use the median of the calculated delays during the calibration period in our calibration process.

2.5 Implementation

We now present the implementation process (fig 2-14). Two process work in parallel. The main process controls the biosignal and detects the point of interest in the incoming biosignal. It runs at the arrival of a 25 data buffer and processes the filtering and the detection algorithm. When it detects a point of interest, it passes it to the other parallel process. This one runs every timestep of the software and controls the signal sent to the microcontroller for the stimulation. At each step of the software, it updates the time and compares it to the timing provided by the main process, which corresponds to the time position of the point of interest plus the constant delay set by the calibration process. It then launches the stimulation and afterward the process controls the simulation duration at each incrementation of the timestep of the software to stop the stimulation after a certain period.
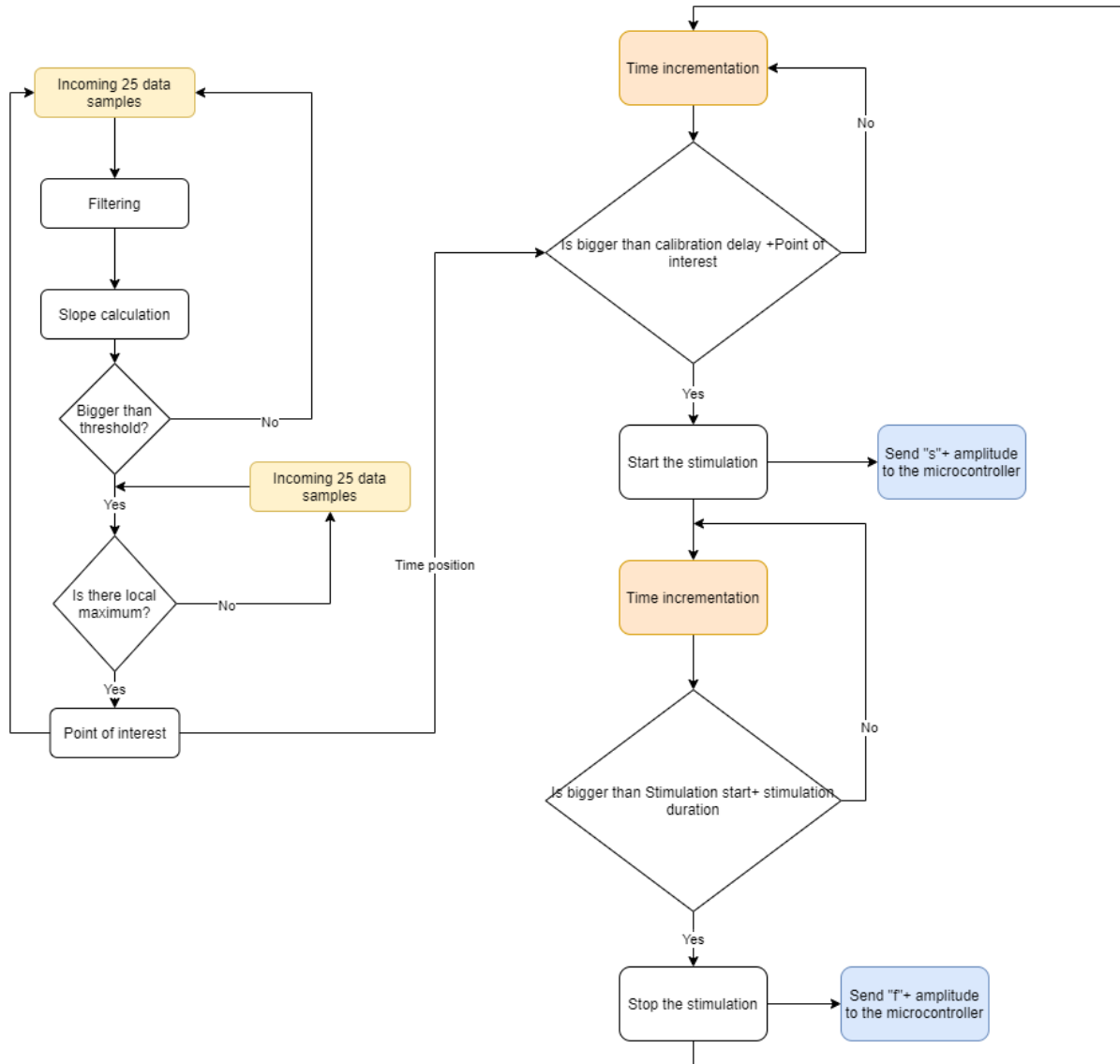
Figure 2-14: Flowchart of the Simulink script.

Simulink

As we state at the beginning, we implemented the whole process in the MATLAB Simulink, see Fig. 2-15.
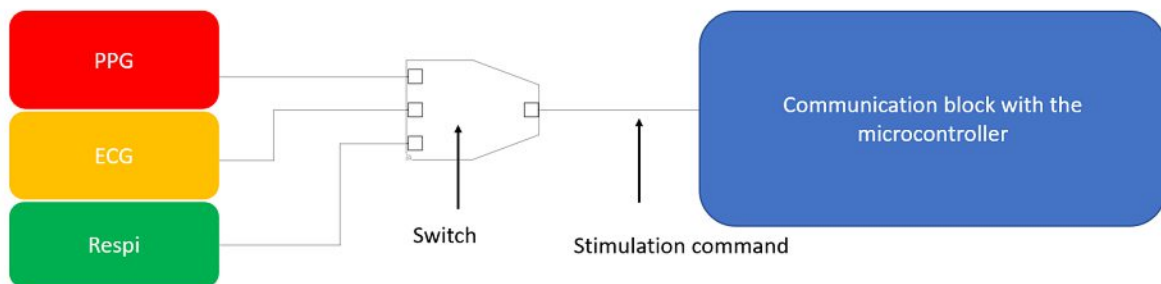
Figure 2-15: Screenshot of the whole Simulink script with schematic.

25

Looking into biosignal processing blocks (PPG, ECG, and Respi), see Fig. 2-16, we can see three sub-blocks, which represent the different processing steps of the biosignal; the left one controls the communication with the NI device to acquire the data (red). The block in the middle makes both the filtering of the data and detect the phase/ point of interest of the corresponding signal (yellow). Finally, the block on the right outputs the stimulation commands depending on what has been detected by the processing block. The stimulation commands are a binary signal: 0 for no stimulation and 1 for stimulation.
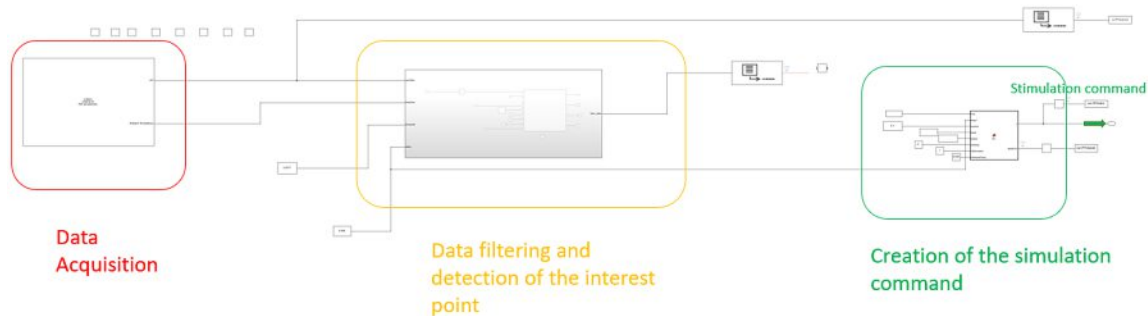
Figure 2-16: subsystems of each processing block.

Graphical User Interface (GUI)

2.5.1.1   General Idea

To improve the stimulation firing system's usability with bio-feedback signals and integrate them, we decided to link a GUI to our Simulink, using a special module provided by Matlab called App designer. This GUI aimed to be able to control the different phases of the stimulation process, change the stimulation parameters, and witness its advancement and precision without having to understand the Simulink code or to use a Matlab postprocessing algorithm. We designed it to be user-friendly for a physician.

Here are the different characteristics of the GUI:

- Control all the phases of the experiment: from the calibration process to the post processing
- Perform the calibration process
- Communication display to guide the user through the different phases
- Display the recorded bio signal and the given stimulation order in real time to witness the good functioning of the process
- Possibility to change the different stimulation parameter in real time without having to stop this
- Possibility to know the precision and the sensitivity of the current session in real time or after the given session
- Possibility to save the bio signal, the stimulation order, and the stimulation parameters for a postprocessing utilization.

2.5.1.2 User guide

When launching the app designer using Matlab, two windows appear: the parameter windows (Fig. 2-17) and the viewing windows:
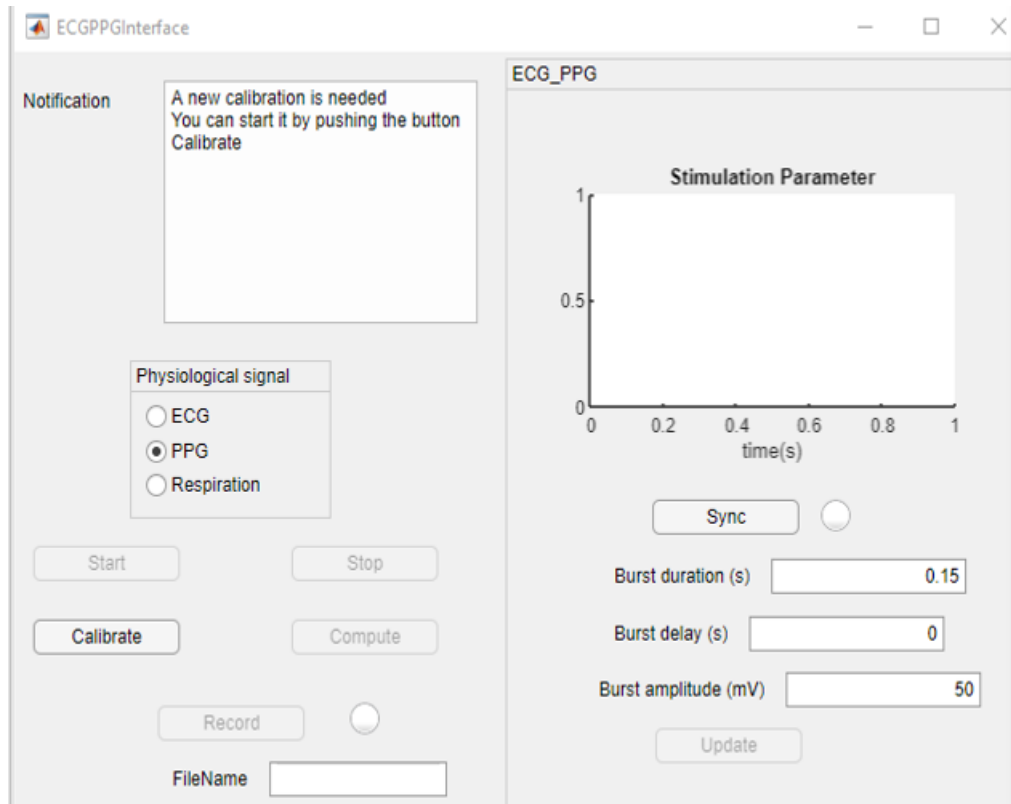
Figure 2-17: GUI app for the control of the stimulation.

The parameter window is the main panel with which the user interacts. It is composed of several elements. At the top left, there is an indication board that indicated the user in which phase of the process he is and which option he has. Left-down, the user can find the general control buttons for the different stimulation phases and the type of biosignal recorded. On the right, a panel for stimulation setting depending on the selected signal and represents the actual stimulation parameters and that the user can change in a certain range.

The logged data panel, which Simulink controlled directly, shows the signals from the Simulink process in real-time. In this window, the user can see the actual biosignal and the corresponding stimulation signal during calibration and stimulation phases.

In general, the type of signal will be selected and run the calibration process. If the acquired signal for 20 seconds is stable enough, the extracted thresholds will be stored for the real-time biosignal processing; otherwise, the calibration process will fail. In both cases, the notification box will announce whether the calibration was successful or failed. A successful calibration enables a synchronized stimulation.

For respiration, there are only two possible parameters: the phase, either inspiration or expiration, and the stimulation amplitude. For the ECG or the PPG, the supervisor can also choose the stimulation duration and the stimulation's starting point for each heart cycle. Those parameters can be changed in real-time during the stimulation.

Once the stimulation is stopped, the stimulation process and the percentage of successful heart cycle detection, and the stimulation's emplacement along each heart cycle can be assessed using the computing button.

2.6 Stimulation

Those detection and prediction processes enable us to approximate the next systolic peak's arrival from the acquired biosignal in Simulink. From this information, we can activate the stimulation as shown in the general schematic. The GUI is connected via serial connection to the microcontroller to turn on or off the stimulation with the given amplitude.

We employed a microcontroller of the STM32 family, which provides many facilities and at the same time a software environment like STM32Cube, which enables a more comfortable programming of the microcontroller. We used an STM32G474xx microcontroller whose characteristic was useful to our specific utilization (Fig. 2-18):

- Numerous advanced analog peripherical, like OpAmp or DAC.
- ADC with 12-bit resolutions
- High-resolution timers
- USART communication

Figure 2-18: STM32G4 family and their characteristics.

Computer-microcontroller communication

Simulink and the microcontroller's communication is done through the USART process with a baud frequency of 115200. Inside the microcontroller, the receiving process is done through the use of DMA in interrupt mode; each time the correct number of bytes is received in the DMA, it triggers a callback function that will change the state of the microcontroller. This DMA signal comprises 3 bytes: the first byte is dedicated to the state command: "s" to start the stimulation and "f" to stop it, and the two other bytes are numerical bytes that command the stimulation amplitude.

Stimulation signal

A tri-phasic stimulation is applied to three electrodes as an output. Each electrode corresponds to one DAC of the microcontroller. They have a relative phase shift to create a virtual ground at the common point if they are connected in a star configuration. Stimulation amplitude is adjusted by GUI and applied to the DAC outputs (Fig. 2-19).
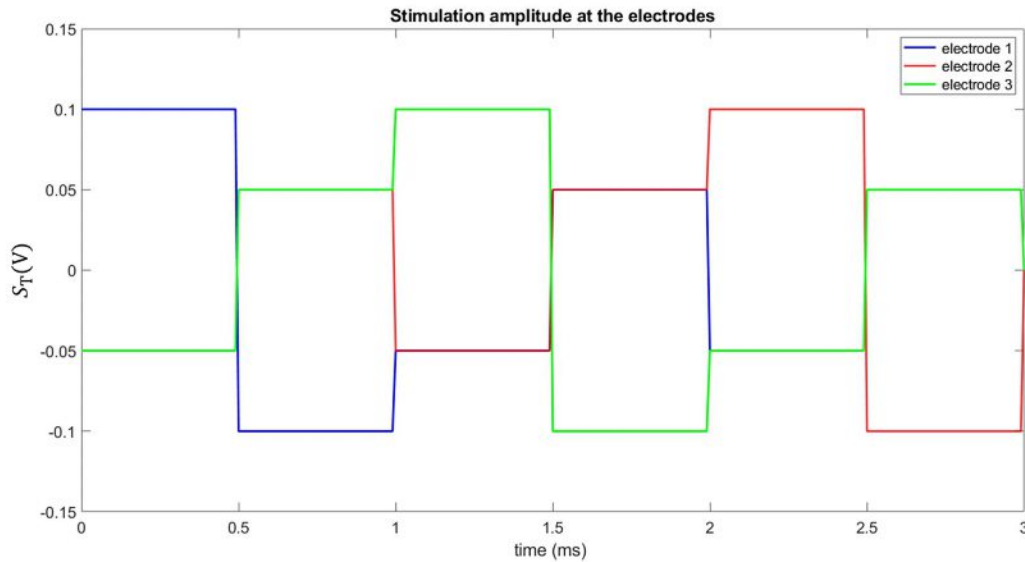
Figure 2-19: Example of the stimulation voltage for 3 electrodes during one cycle.

3 Results

3.1 Optimization of the calibration

The detection process's performance depends significantly on the calibration process and how it represents the whole signal. Moreover, it depends on the selected threshold level from the calibration phase for R-peak (ECG) or systolic phase (PPG) slope. Hence, we examined a 120s ECG signal to verify the detection process, depending on this selected threshold. We used the first 20 seconds of this signal to perform the calibration process. Here is the distribution of the R-peak slopes (Fig. 3-1).
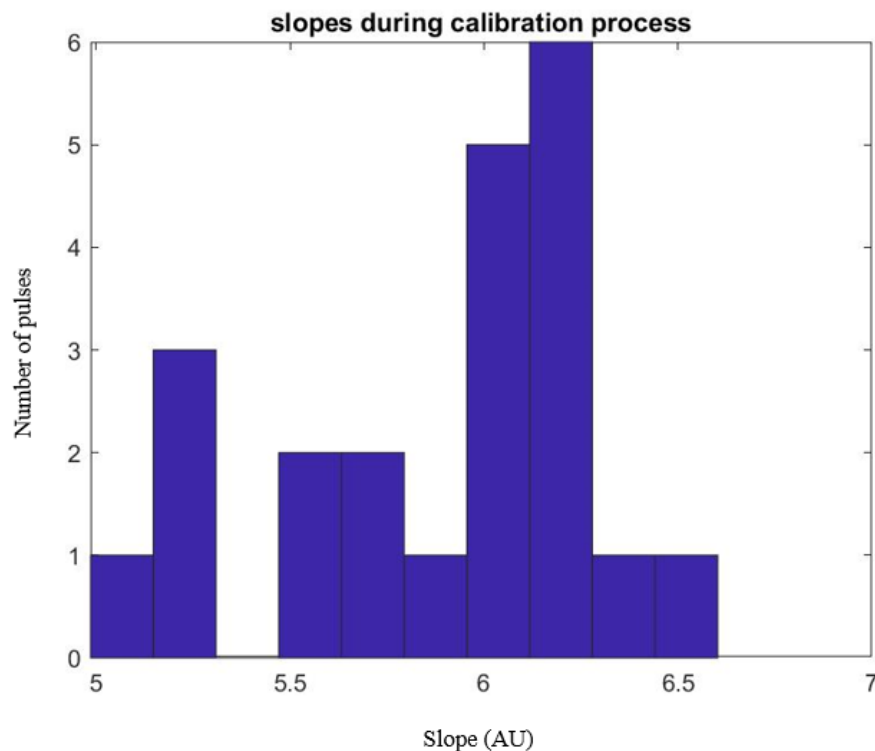
Figure 3-1: Slope distribution for a training set of ECG pulses.

We can see that there is no outlier thanks to the incoming signal, which is quite regular, it would have been then possible to take the minimum of those slopes. Then, we check the impact of the downscaling factors on the number of detected R peak: We computed the sensitivity: the number of correctly detected peaks over the total number of peaks, in the whole training set for different values of the downscaling factor from 10% to 100% (Fig. 3-2).
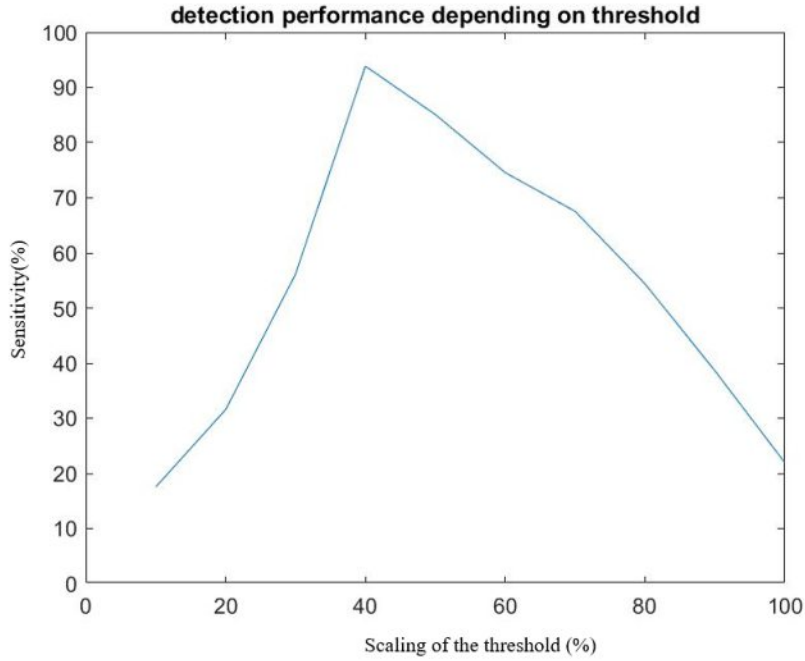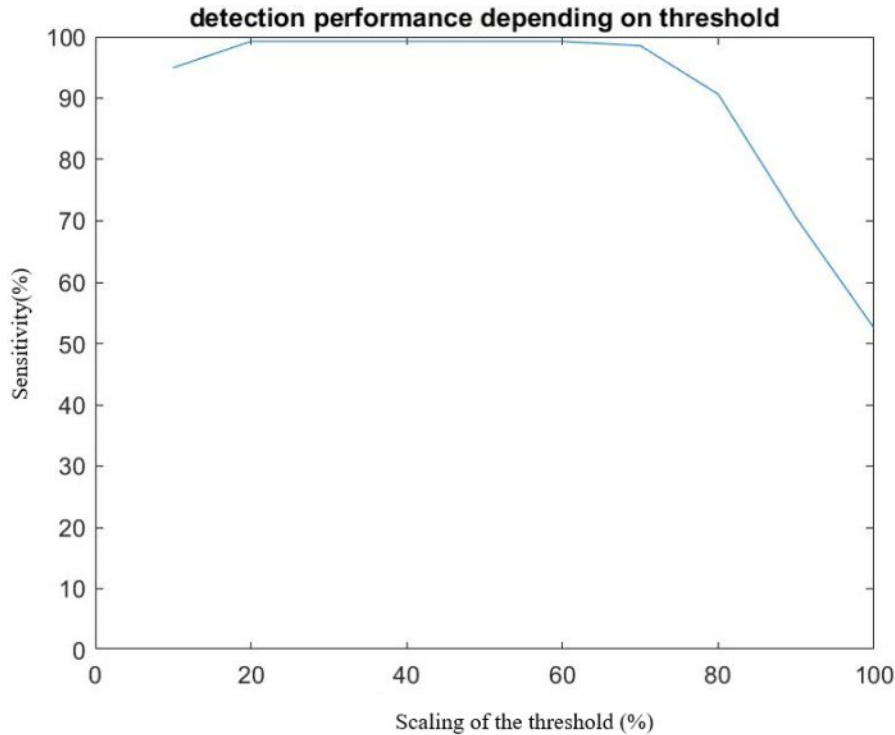
Figure 3-2: Sensitivity, percentage of correctly detected R peaks over the total number of R peak in the signal, depending on the threshold scaling for a training set of ECG pulses.

To have a wider number of samples, we did the experiment twice with the same duration, 120s (Fig. 3-3).
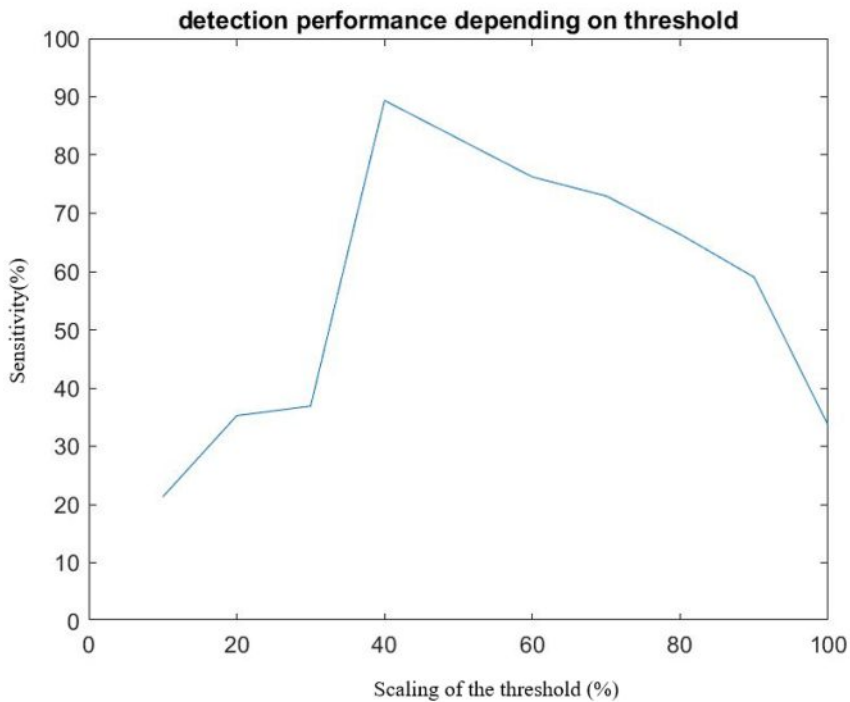
Figure 3-3: Sensitivity, percentage of correctly detected R peaks over the total number of R peak in the signal, depending on the threshold scaling for a training set of ECG.

We can see that the best downscaling factor for the slope threshold level is the same and around 40% in both cases. Another interesting point of the two graphs is that the performance decreases when reducing the threshold under a specific value. The effect is due to the detection of other peaks, like T-peak, which prevents the subsequent R peak detection due to a "refraction period" of the detection process. We have a reasonable detection rate with such a process, depending on the threshold's calibration accuracy.

We examined the PPG calibration process similarly, which yields a similar slope distribution as ECG (Fig. 3-4).
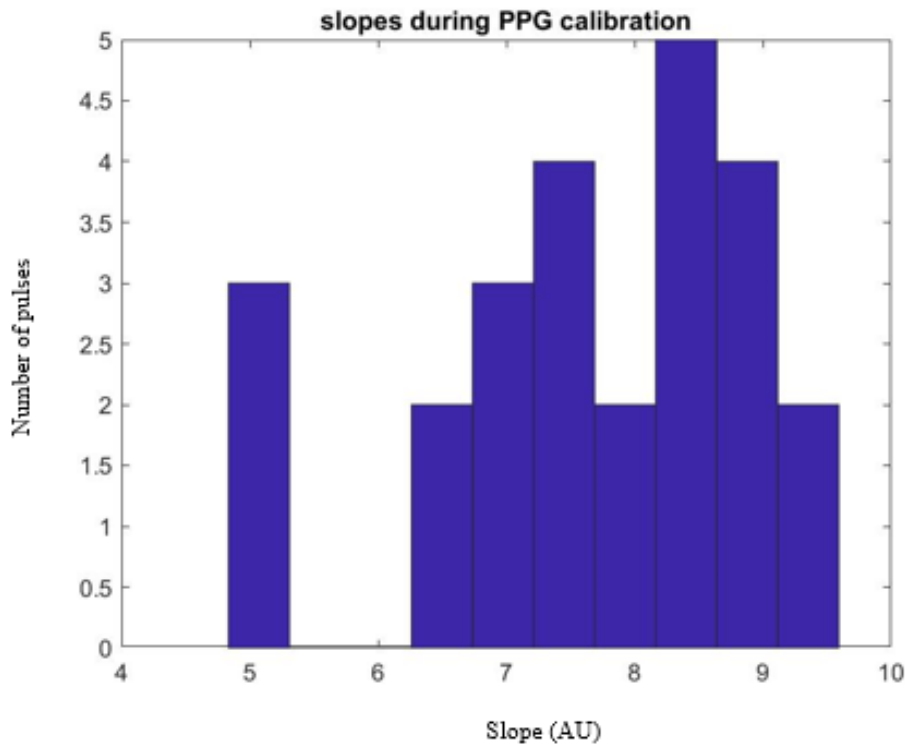
Figure 3-4: Slope distribution for a training set of PPG pulses.

However, for the PPG threshold calibration, due to the waveform difference compared to the ECG, the sensitivity will not be affected for lower thresholds, which means that the other peaks either do not exist or are less prominent to be detected as false peaks (Fig. 3-5).

Figure 3-5: Sensitivity, percentage of correctly detected systolic peaks over the total number of systolic peak in the signal depending on the threshold scaling for a training set of PPG pulses.

Therefore, a downscale factor of 40% for the threshold level like the ECG provides an acceptable pulse detection.

3.2 Validation of the detection process on a test set

To validate the detection method and obtained threshold levels by the calibration process, we examined another dataset from the EUROBAVAR study, which has the advantage of providing both ECG and PPG data with a duration of approximately 10 minutes and 500 Hz sampling frequency.

Each data set was fed into the Simulink to mimic the real-time process. We took the first 20s to perform the calibration process and the threshold determination, and then we fed the signal as in real-time, taking 25 data sample frames every 50 ms to perform the threshold comparison. Actual and real-time detected R-peaks and systolic peaks were compared to evaluate the method's sensitivity and specificity (Table 3-1).

- The sensitivity: the number of well detected peaks divided by the whole number of peaks in the signal.
- The specificity: the number of well detected peaks divided by the whole number of peaks detected by our algorithm.

Table 3-1: Results of the point of interest detection on EUROBAVAR data set

		ECG		PPG	
		Se	Sp	Se	Sp
A002	Standing	0.972	0.997	0.999	0.998
	Laying	1	1	1	0.998
A003	Standing			0.981	0.979
	Laying			0.961	0.959
A006	Standing	0.928	0.984	1	0.999
	Laying	0.985	0.991	1	0.998
B002	Standing	0.983	0.999	0.998	0.998
	Laying	0.993	0.997	0.997	0.995
B006	Standing	0.927	0.996	0.979	0.978
	Laying	0.918	0.999	0.974	0.974

For most of the data sample, we have a sensitivity and specificity higher than 95%, which is close to what it obtained with other detecting algorithms. For the A003, we did not provide any data for the ECG, as the signal showed the differential of ECG instead of the ECG.

3.3 Validation of the stimulation timing

To assess the platform's performance in real-time, we performed an in-vitro test to evaluate the real delay between the biosignal coming from the body, detected point of the interest (R-peak, systolic peak, or diastolic valley), and the stimulation firing time via serial connection.

We first made a qualitative test where we visually compared the biosignal output from the Biopac station to the A/D converter and the output of the stimulation from the microcontroller at the same time on two channels of an oscilloscope. We observed a delay between the two signals. Whereas this delay would completely invalidate our approach in case of a direct stimulation process, the more flexible predictive stimulation provides tools to bypass the undesired delay.

Main idea

The advantage of using a predictive stimulation approach is that we can accept an arbitrary delay due to processing and device communication by compensating it in the stimulation command. Hence, we investigated this delay quantitatively; we observed that this delay mainly originates from two different places:

- a time delay between the input signal of the Biopac and Simulink.

- stimulation command between the output signal in Simulink and the actual stimulation at the outside of the microcontroller.

Delays summarized in the following schematic of the whole platform and systematic delays are highlighted (Fig. 3-6)
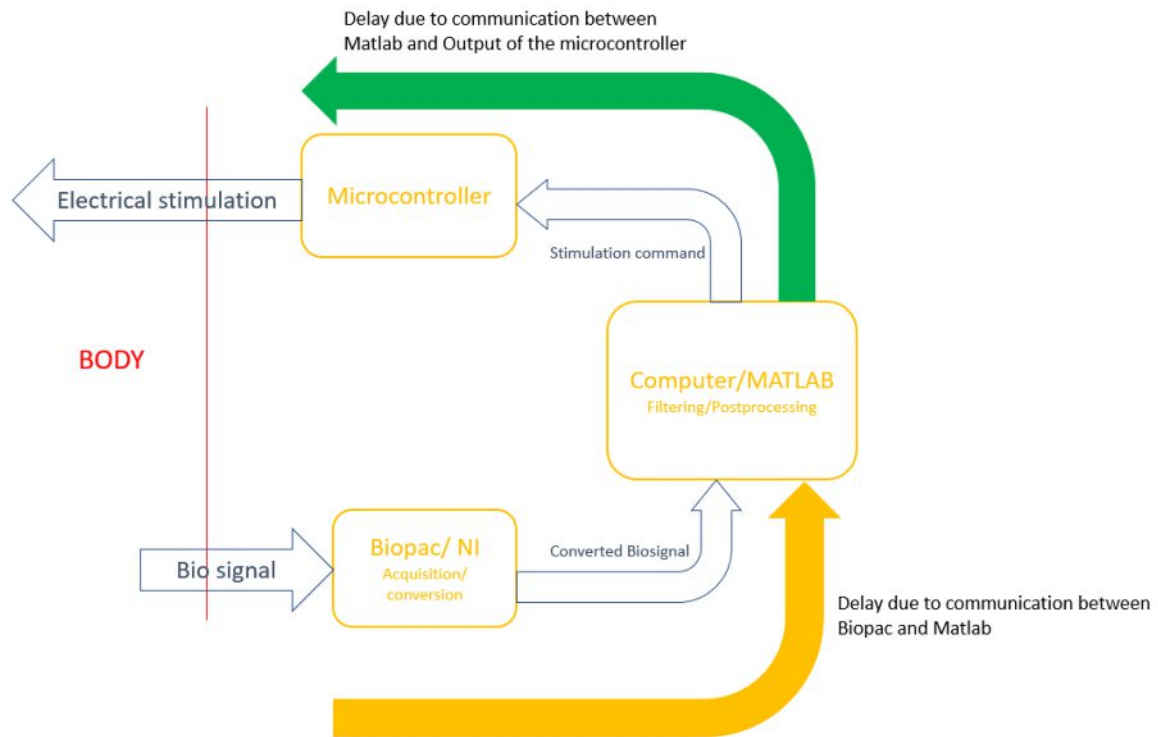
:

Figure 3-6: Schematic of the platform with highlighted systematic delays.

We then designed an experiment to know the undesired delay of the whole system, which is the sum of the two delays that we showed on the schematic by the yellow and green arrows. To assess this, we closed the loop of our system and recorded the final stimulation signal with another channel of the Biopac along with the biosignal for two minutes. We then have 4 different signals in two softwares with their own timing. In the Biopac software, we have the incoming biosignal from the biosensor, which is the real time signal from the patient and the real time stimulation signal from the microcontroller, and in Simulink the transmitted biosignal that we process and the stimulation command that derives from this process. The Figure 3-7 shows all the different signals. The different delays are highlighted on the figure:

-The **communication delays** that we want to calculate in yellow and in green.

- The **visible delays** that corresponds to the delay between the interesting point of the biosignal and the following beginning of a stimulation period from the stimulation command in the same software. We then have 2 visible delays, one in Simulink and one in the BIOPAC software.
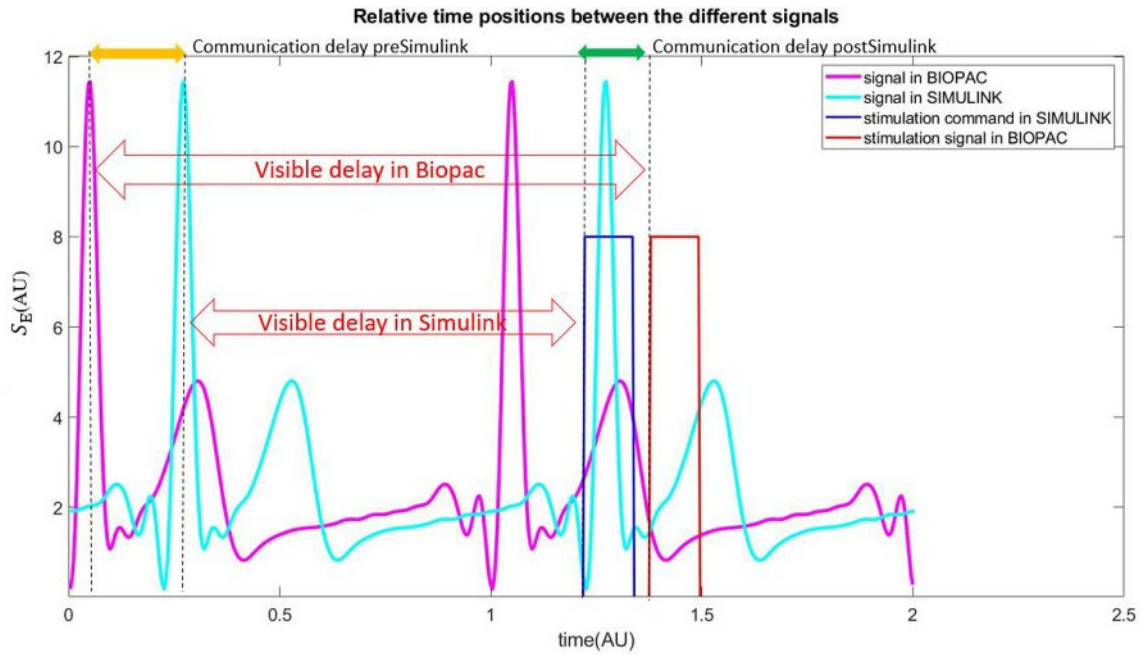
Figure 3-7: Sum up of the different signals during the experiment with their respective position in time.

Once the experiment was performed, the data from the Biopac software were post-processed in MATLAB, and the delay distribution between the onset of the stimulation and R-peak of the acquired data at Biopac calculated to get what we called the visible delay in Biopac, we then subtract the visible delay in Simulink ,whose value is constant and comes from the calibration process . Finally, the obtained delay is the total delay (yellow and green) due to the Biopac conversion, ADC and Simulink processing, and serial communication between Simulink and the microcontroller. Its distribution is presented in Figure 3-8.
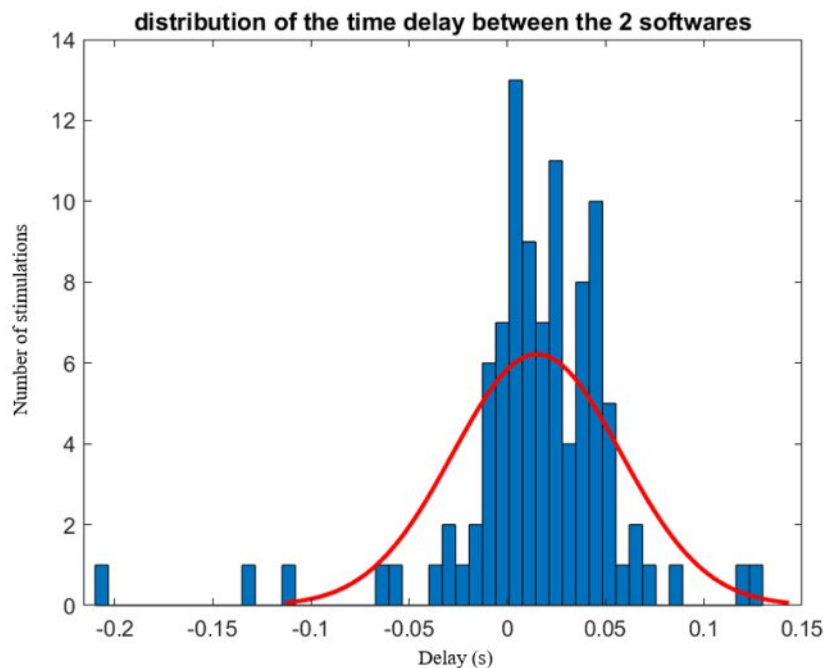
Figure 3-8: Result of the total delay showing the delay distribution before correction.

This positive delay can be considered in Simulink while creating the stimulation command order to get a real stimulation closer to the real point of interest. Figure 3-9 shows how this correction shifts the delay to the zero.
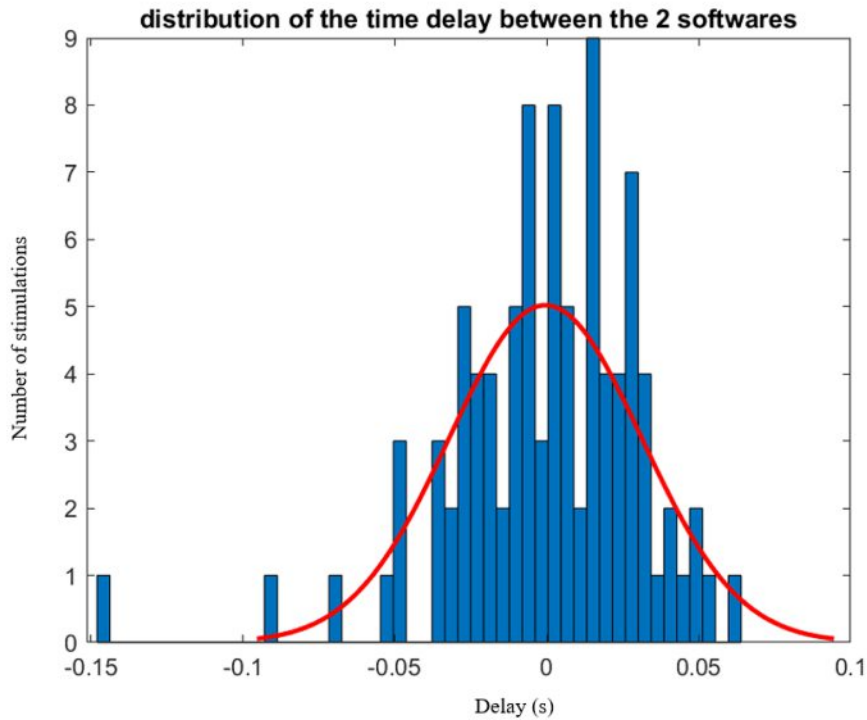
Figure 3-9: corrected systemic delay.

The mean value of the delay distribution is zero with a standard deviation of 20ms, which is acceptable to target any point in the heart cycle. Comparing to the systemic delay, which causes a delay of 100ms and could the precision of the triggering point based on the heart cycle's event, removal of this delay with 20 ms standard deviation profound the stimulation with bio-feedback.

3.4   Simulation performance review

Although we did not perform any real stimulation for this thesis, and it is difficult to foresee the effect that such stimulation will have on the CVS, we could nevertheless assess the performance of the platform in term of target stimulation. The GUI, besides controlling the stimulation, provides an integrated mean to witness the platform's performance in real-time and to observe the position of the stimulation concerning the cardiovascular cycle of the patient.

 Indeed, after the stimulation session a post processing step of the recorded bio signal during the stimulation session takes place and consistes in the detection of each heart cycle, their normalization between 0 and 1 both in time and in amplitude, and their resampling into 256 points. Such a normalization enables to have a brief overview over the patient bio signal, as well as to sum up the stimulation timing over the whole session.

The various experiments that we made confirmed the robustness of our platform, both in term of biosignal detection and stimulation timing in the cardiovascular cycle (Fig 3-10).
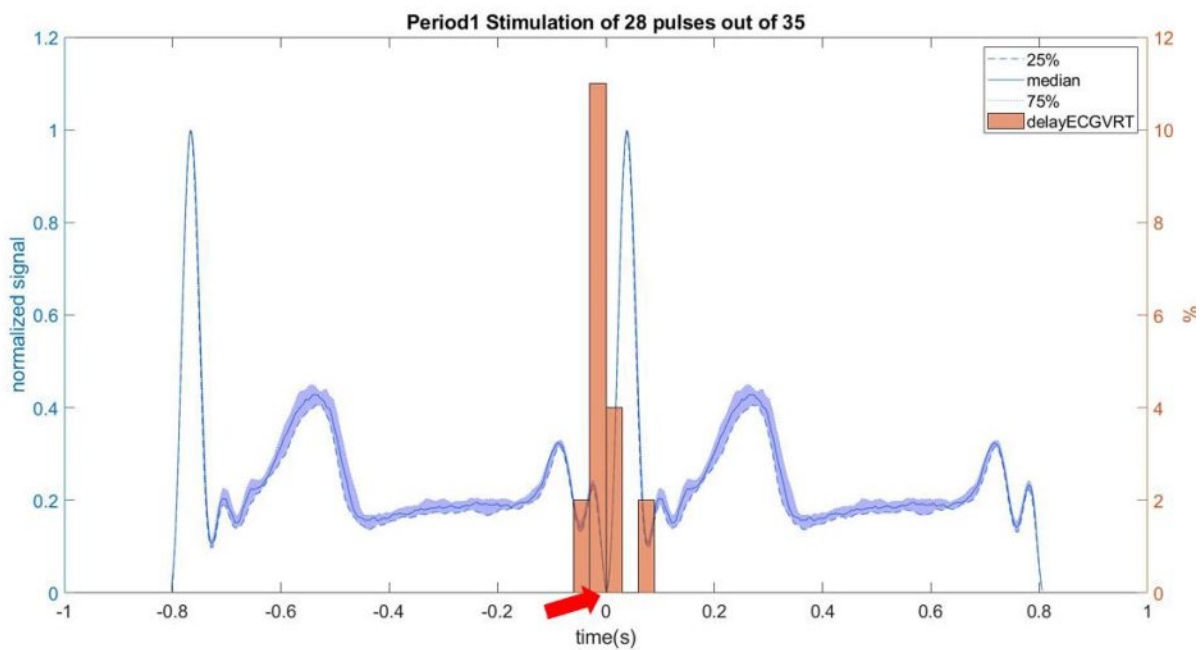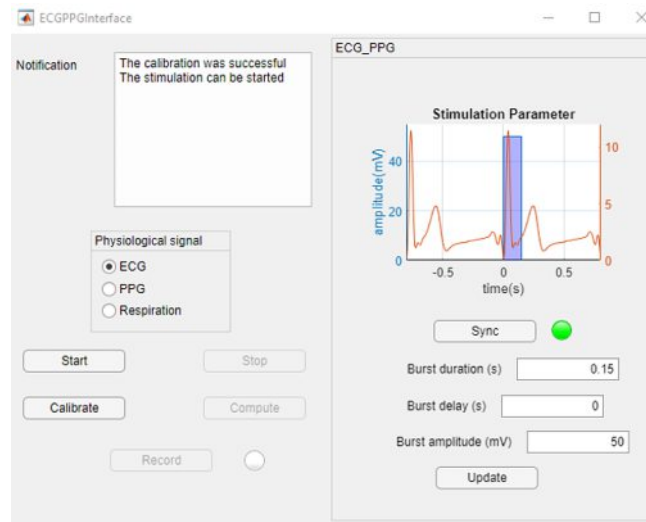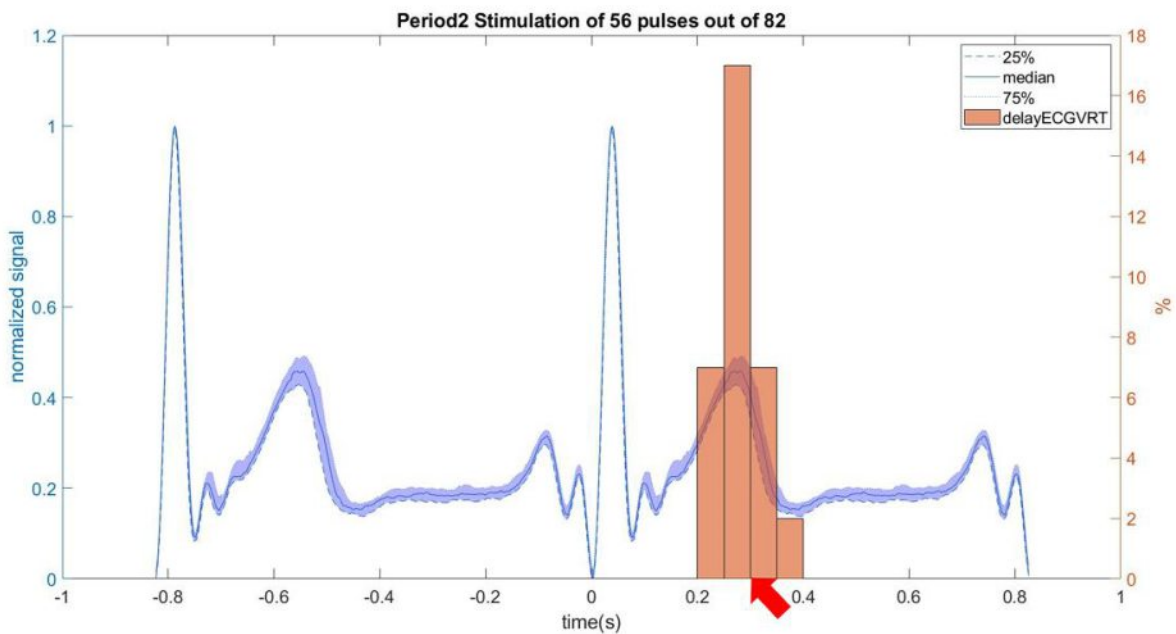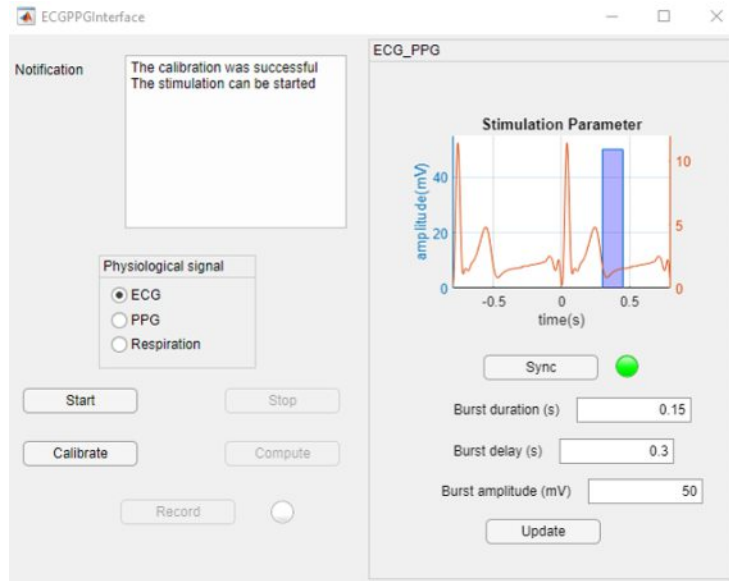

Figure 3-10: Result of an ECG experiment for 28s.Top: GUI showing the setting. Bottom: Computational plot for a 28s stimulation session. Over the stimulation session, the ECG biosignal has been segmented using the Q peaks, each segment has then been normalized between 0 and 1 in the Y axis and 0 and the mean period in the X axis. Finally those normalized segments have been resampled with 256 points. The blue plots show the distribution of the biosignal for each of the 256 points. The red arrow shows the target of the stimulation.

On the plot provided by the GUI, we can witness both the general form of the patient biosignal (blue) and the distribution of localization of the beginning of the stimulation phase (red). In the experiment shown above, which lasted 28 seconds after the calibration phase, the chosen target of the stimulation was the beginning of the QRS complex, and we can notice the statistical distribution around this target point. As explained before, the platform also offers the possibility to vary the stimulation target (Fig 3-11).

Figure 3-11: Result of an ECG experiment for 65s. Top: GUI showing the setting. Bottom: Computational plot for a 65s experiment with a given stimulation target. Over the stimulation session, the ECG biosignal has been segmented using the Q peaks, each segment has then been normalized between 0 and 1 in the Y axis and 0 and the mean period in the X axis. Finally those normalized segments have been resampled with 256 points. The blue plots show the distribution of the biosignal for each of the 256 points. The red arrow shows the target of the stimulation.

This possibility to witness the accuracy of the stimulation is also offered for the PPG, due to the similar stimulation process (Fig. 3-12):
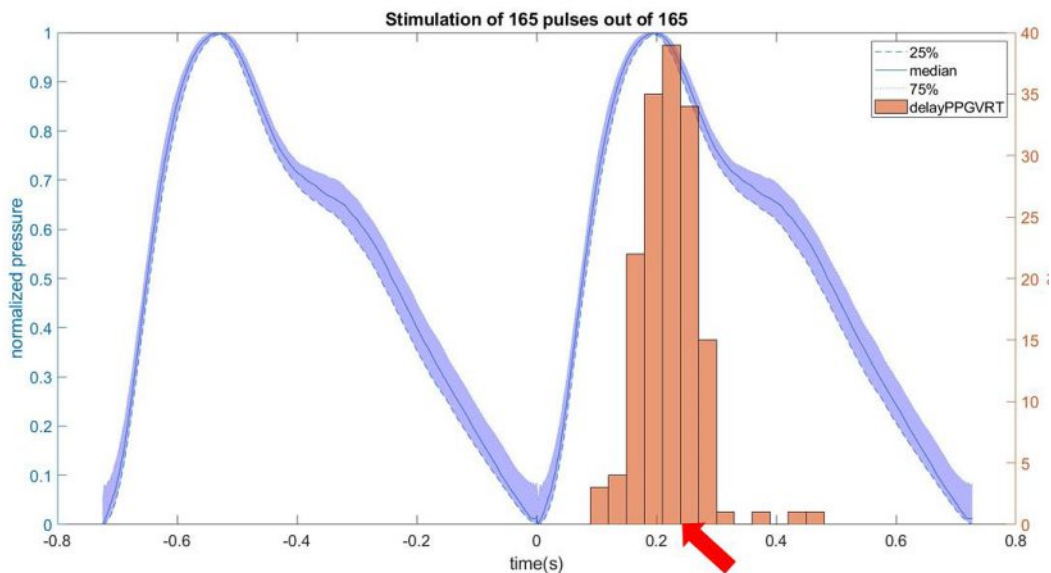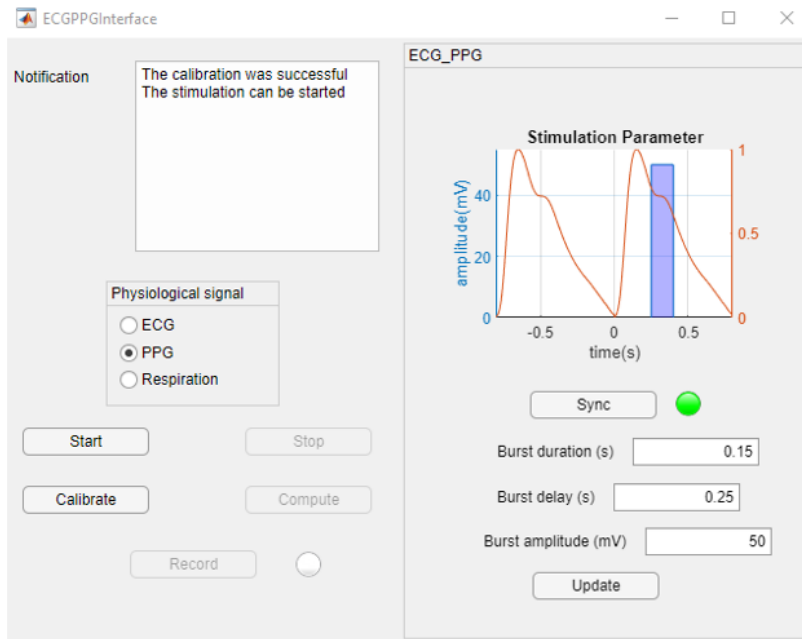
Figure 3-12: Result of an PPG experiment for 120s. Top: GUI showing the setting. Bottom: The PPG biosignal has been segmented using the diastolic peak. Each segment has then been normalized and resampled into 256 points. The plotted distributions curves shows the distribution for each 256 points. The red arrow represent the stimulation target.

Those plots help to follow the performance of the stimulation device to later correlate them to the patient response to the stimulation. For the respiratory driven stimulation, due to the slower time constant, the Simulink Data Inspector seems enough to monitor the stimulation process.

4 Discussions

The developed platform provides a flexible setting for stimulation parameters, bio-feedback type selection, and adaptation to the subject biosignal. A reasonable error of detection due to the heart rate variability provides a robust experimental setup to investigate the effect of aVNS based on the heart cycle events. Although the point of interest for stimulation is delayed by one heart cycle, in terms of the cardiovascular system, response due to the stimulation is promising. The dependency of the precision of the point of the interest could increase the error of estimation for higher HRV and vice versa for the lower HRV. The calibration process is the base of the real-time process of the acquired data; therefore, a successful calibration phase would cover the signal fluctuation due to the sensor and electrodes' quality. Moreover, deep breathing over the calibration process would cover variabilities due to respiration.

Immediate data analysis of the acquired biosignal with/without stimulation would show the percentage of the succeeded stimulation over the targeted point and the whole number of experimented pulses. Therefore, the experimenter can control the whole process of the stimulation not to have irrelevant results. Moreover, a real-time presentation of stimulation and acquired biosignal enables a visual overview of the event's coincidences.

This platform provides a base to analyze the aVNS effect on the cardiovascular system, especially baroreflex activity in response to the elevated parasympathetic tone—moreover, a foundation to personalizing aVNS based on the sympathetic or parasympathetic contribution on the CVS. A more efficient and adaptive aVNS would be the aim of this platform.

Regarding the incoming revolution of personalized medicine, this stimulation of the vagal nerve at specific moments of the cardiovascular cycle, if conclusive, could be adapted to each patient as long as other parameters to maximize the positive effects of the stimulation on the patient health. The lightness of the aVNS process with no invasive operation to install the electrodes would make it suitable for the patient's autodidact use in his everyday life in an embedded device.

5 Appendix

5.1 Movement artifact detection

As we mentioned in the methodology part, we tried to implement a movement artefact detection for PPG, based on pulse recognition [38] and is done through the calculation of the cross-correlation coefficient between the pulse that we want to classify and a template which is taken as the first principal component of a set of well-defined training pulses.

Methodology

In the following, we will explain how we adapted this process to a real-time process in Simulink.

For each 1000 incoming data samples, which represent approximately 2s and in which we expect to find at least one complete pulse, we filter the data with the same lowpass filter as for the main algorithm, then we use a find peaks on the opposite of the signal to find the diastolic minimums, and we select the data between the two last ones which we expect to be the last pulse.

The next step is to process this data to compare it to the template. Hence, we rescale the X- and Y-axis between the 0 and 1 both, and we resample the data into 256 points. We then calculate the cross-correlation coefficient between the given pulse and the template and compare it to the predefined threshold: If it is bigger, we admit that the pulse has the correct form and that there is no movement artifact; on the contrary, if the coefficient is smaller than the threshold, there are movement artefacts, and we stop the stimulation until that we recognize a good pulse.

Results

We tested this algorithm manually and in real-time by witnessing the advance of the biosignal and by creating at a certain point a movement artefact by moving the finger on which the PPG biosensor was attached in a particular direction to create a change in the PPG biosignal.
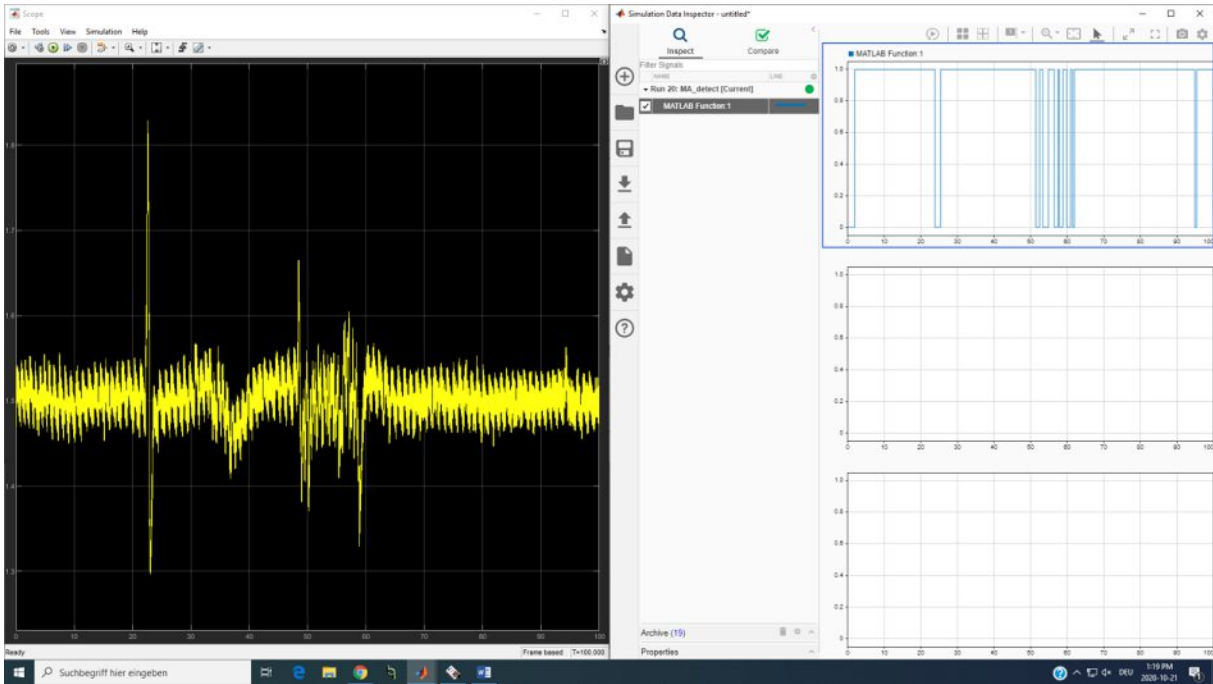
Figure 5-1: Screenshot of the PPG MA detection showing both the rough signal on the left and the detection outcome on the right

In the previous figure, we can see on the left a 100 seconds PPG signal with three major movement artefacts that make the signal unreadable for the stimulation. The algorithm correctly detects the first one around 25th second, the last one around 95th second. Otherwise, the period between 50 and 60s is more complicated, and we do not make any stimulation during this period.

List of References

1 Rutecki P. *Anatomical, physiological, and theoretical basis for the antiepileptic effect of vagus nerve stimulation*. Epilepsia. 1990;31 Suppl 2:S1-6. doi: 10.1111/j.1528-1157.1990.tb05843.x. PMID: 2226360.

2 Connor DE Jr, Nixon M, Nanda A, Guthikonda B. *Vagal nerve stimulation for the treatment of medically refractory epilepsy: a review of the current literature*. Neurosurg Focus. 2012 Mar;32(3):E12. doi: 10.3171/2011.12.FOCUS11328. PMID: 22380853.

3 Johnson RL, Wilson CG. A *review of vagus nerve stimulation as a therapeutic intervention*. J Inflamm Res. 2018 May 16;11:203-213. doi: 10.2147/JIR.S163248. PMID: 29844694; PMCID: PMC5961632.

4 Kaniusas E, Kampusch S, Tittgemeyer M, Panetsos F, Gines RF, Papa M, Kiss A, Podesser B, Cassara AM, Tanghe E, Samoudi AM, Tarnaud T, Joseph W, Marozas V, Lukosevicius A, Ištuk N, Šarolić A, Lechner S, Klonowski W, Varoneckas G, Széles JC. *Current Directions in the Auricular Vagus Nerve Stimulation I - A Physiological Perspective*. Front Neurosci. 2019 Aug 9;13:854. doi: 10.3389/fnins.2019.00854. PMID: 31447643; PMCID: PMC6697069.

5 Ay I, Napadow V, Ay H. Electrical stimulation of the vagus nerve dermatome in the external ear is protective in rat cerebral ischemia. Brain Stimul. 2015 Jan-Feb;8(1):7-12. doi: 10.1016/j.brs.2014.09.009. Epub 2014 Sep 28. PMID: 25312600; PMCID: PMC4277719.

6 Koopman FA, van Maanen MA, Vervoordeldonk MJ, Tak PP. Balancing the autonomic nervous system to reduce inflammation in rheumatoid arthritis. J Intern Med. 2017 Jul;282(1):64-75. doi: 10.1111/joim.12626. Epub 2017 May 26. PMID: 28547815.

7 Redgrave J, Day D, Leung H, Laud PJ, Ali A, Lindert R, Majid A. Safety and tolerability of Transcutaneous *Vagus Nerve stimulation in humans; a systematic review*. Brain Stimul. 2018 Nov-Dec;11(6):1225-1238. doi: 10.1016/j.brs.2018.08.010. Epub 2018 Aug 23. PMID: 30217648.

8 Badran BW, Mithoefer OJ, Summer CE, LaBate NT, Glusman CE, Badran AW, DeVries WH, Summers PM, Austelle CW, McTeague LM, Borckardt JJ, George MS. *Short trains of transcutaneous auricular vagus nerve stimulation (taVNS) have parameter-specific effects on heart rate*. Brain Stimul. 2018 Jul-Aug;11(4):699-708. doi: 10.1016/j.brs.2018.04.004. Epub 2018 Apr 6. PMID: 29716843; PMCID: PMC6536129.

9 Mahadi KM, Lall VK, Deuchars SA, Deuchars J. Cardiovascular autonomic effects of transcutaneous auricular nerve stimulation via the tragus in the rat involve spinal cervical sensory afferent pathways. Brain Stimul. 2019 Sep-Oct;12(5):1151-1158. doi: 10.1016/j.brs.2019.05.002. Epub 2019 May 6. PMID: 31129152.

10 Annoni EM, Xie X, Lee SW, et al. Intermittent electrical stimulation of the right cervical vagus nerve in salt-sensitive hypertensive rats: effects on blood pressure, arrhythmias, and ventricular electrophysiology. Physiological Reports. 2015 Aug;3(8). DOI: 10.14814/phy2.12476. PMID: 26265746 ; PMCID: PMC4562562

11 De Ferrari GM, Crijns HJ, Borggrefe M, Milasinovic G, Smid J, Zabel M, Gavazzi A, Sanzo A, Dennert R, Kuschyk J, Raspopovic S, Klein H, Swedberg K, Schwartz PJ; CardioFit Multicenter Trial Investigators. Chronic vagus nerve stimulation: a new and promising therapeutic approach for chronic heart failure. Eur Heart J. 2011 Apr;32(7):847-55. doi: 10.1093/eurheartj/ehq391. Epub 2010 Oct 28. PMID: 21030409.

12 E. Kaniusas, S. Kampusch and J. C. Szeles, "Depth profiles of the peripheral blood oxygenation in diabetics and healthy subjects in response to auricular electrical stimulation: Auricular vagus nerve stimulation as a potential treatment for chronic wounds," 2015 IEEE Sensors Applications Symposium (SAS), Zadar, Croatia, 2015, pp. 1-6, doi: 10.1109/SAS.2015.7133566.

13 Yap JYY, Keatch C, Lambert E, Woods W, Stoddart PR, Kameneva T. Critical *Review of Transcutaneous Vagus Nerve Stimulation: Challenges for Translation to Clinical Practice*. Front Neurosci. 2020 Apr 28; 14:284. doi: 10.3389/fnins.2020.00284. PMID: 32410932; PMCID: PMC7199464.

14 Yakunina N, Kim SS, Nam EC. *Optimization of Transcutaneous Vagus Nerve Stimulation Using Functional MRI*. Neuromodulation. 2017 Apr;20(3):290-300. doi: 10.1111/ner.12541. Epub 2016 Nov 29. PMID: 27898202.

15 Rattay, Frank & Greenberg, R.J. & Resatz, Susanne. (2002). *Neuron modeling*. Handbook of Neuroprosthetic Methods. 39-71. 10.1201/9781420040876.ch3.

16 Samoudi AM, Kampusch S, Tanghe E, Széles JC, Martens L, Kaniusas E, Joseph W. *Numerical modeling of percutaneous auricular vagus nerve stimulation: a realistic 3D model to evaluate sensitivity of neural activation to electrode position*. Med Biol Eng Comput. 2017 Oct;55(10):1763-1772. doi: 10.1007/s11517-017-1629-7. Epub 2017 Feb 13. PMID: 28194649.

17 Eugenijus Kaniusas*, Biomedical Signals and Sensors I: Linking physiological phenomena and biosignals*, Springer Publisher (2012)

18 Srinivasan R, Nudelman HB. *Modeling the carotid sinus baroreceptor*. Biophys J. 1972 Sep;12(9):1171-82. doi: 10.1016/S0006-3495(72)86153-8. PMID: 5056961; PMCID: PMC1484137.

19 Chapleau MW, Abboud FM. *Contrasting effects of static and pulsatile pressure on carotid baroreceptor activity in dogs*. Circ Res. 1987 Nov;61(5):648-58. doi: 10.1161/01.res.61.5.648. Erratum in: Circ Res 1988 Jul;63(1):272. PMID: 3664974.

20 Min S, Chang RB, Prescott SL, Beeler B, Joshi NR, Strochlic DE, Liberles SD. *Arterial Baroreceptors Sense Blood Pressure through Decorated Aortic Claws*. Cell Rep. 2019 Nov 19;29(8):2192-2201.e3. doi: 10.1016/j.celrep.2019.10.040. PMID: 31747594; PMCID: PMC6893869.

21 Brown HF, Kimura J, Noble D, Noble SJ, Taupignon A. *The ionic currents underlying pacemaker activity in rabbit sino-atrial node: experimental results and computer simulations*. Proc R Soc Lond B Biol Sci. 1984 Sep 22;222(1228):329-47. doi: 10.1098/rspb.1984.0067. PMID: 6149555.

22 Jalife J, Slenter VA, Salata JJ, Michaels DC. *Dynamic vagal control of pacemaker activity in the mammalian sinoatrial node*. Circ Res. 1983 Jun;52(6):642-56. doi: 10.1161/01.res.52.6.642. PMID: 6861283.

23 Kawada T, Sugimachi M. *Open-loop static and dynamic characteristics of the arterial baroreflex system in rabbits and rats*. J Physiol Sci. 2016 Jan;66(1):15-41. doi: 10.1007/s12576-015-0412-5. Epub 2015 Nov 5. PMID: 26541155; PMCID: PMC4742515

24 Ursino M. *Interaction between carotid baroregulation and the pulsating heart: a mathematical model*. Am J Physiol. 1998 Nov;275(5):H1733-47. doi: 10.1152/ajpheart.1998.275.5.H1733. PMID: 9815081.

25 Ursino M, Magosso E. *Acute cardiovascular response to isocapnic hypoxia. I. A mathematical model*. Am J Physiol Heart Circ Physiol. 2000 Jul;279(1):H149-65. doi: 10.1152/ajpheart.2000.279.1.H149. PMID: 10899052.

26 Berteotti C, Franzini C, Lenzi P, Magosso E, Ursino M, Zoccoli G, Silvani A. *The baroreflex contribution to spontaneous heart rhythm assessed with a mathematical model in rats*. Auton Neurosci. 2008 Feb 29;138(1-2):24-30. doi: 10.1016/j.autneu.2007.09.003. Epub 2007 Oct 22. PMID: 17936694.

27 Silvani A, Magosso E, Bastianini S, Lenzi P, Ursino M. *Mathematical modeling of cardiovascular coupling: Central autonomic commands and baroreflex control*. Auton Neurosci. 2011 Jul 5;162(1-2):66-71. doi: 10.1016/j.autneu.2011.04.003. Epub 2011 May 8. PMID: 21550860.

28 Butt MF, Albusoda A, Farmer AD, Aziz Q. *The anatomical basis for transcutaneous auricular vagus nerve stimulation*. J Anat. 2020 Apr;236(4):588-611.

doi: 10.1111/joa.13122. Epub 2019 Nov 19. PMID: 31742681; PMCID: PMC7083568.

29 Mifflin SW, Spyer KM, Withington-Wray DJ. *Baroreceptor inputs to the nucleus tractus solitarius in the cat: postsynaptic actions and the influence of respiration*. J Physiol. 1988 May;399:349-67. doi: 10.1113/jphysiol.1988.sp017085. PMID: 3404463; PMCID: PMC1191669.

30 Mastitskaya S, Turovsky E, Marina N, Theparambil SM, Hadjihambi A, Kasparov S, Teschemacher AG, Ramage AG, Gourine AV, Hosford PS. *Astrocytes Modulate Baroreflex Sensitivity at the Level of the Nucleus of the Solitary Tract*. J Neurosci. 2020 Apr 8;40(15):3052-3062. doi: 10.1523/JNEUROSCI.1438-19.2020. Epub 2020 Mar 4. PMID: 32132265; PMCID: PMC7141885.

31 Dampney RA. *Functional organization of central pathways regulating the cardiovascular system*. Physiol Rev. 1994 Apr;74(2):323-64. doi: 10.1152/physrev.1994.74.2.323. PMID: 8171117.

32 Gourine AV, Machhada A, Trapp S, Spyer KM. *Cardiac vagal preganglionic neurones: An update*. Auton Neurosci. 2016 Aug;199:24-8. doi: 10.1016/j.autneu.2016.06.003. Epub 2016 Jul 1. PMID: 27396874.

33 Raven PB, Fadel PJ, Ogoh S. *Arterial baroreflex resetting during exercise: a current perspective*. Exp Physiol. 2006 Jan;91(1):37-49. doi: 10.1113/expphysiol.2005.032250. Epub 2005 Oct 6. PMID: 16210446.

34 Blanchard S, Saillet S, Ivanov A, Benquet P, Bénar CG, Pélégrini-Issac M, Benali H, Wendling F. *A New Computational Model for Neuro-Glio-Vascular Coupling: Astrocyte Activation Can Explain Cerebral Blood Flow Nonlinear Response to Interictal Events*. PLoS One. 2016 Feb 5;11(2):e0147292. doi: 10.1371/journal.pone.0147292. PMID: 26849643; PMCID: PMC4743967.

35 Jansen BH, Zouridakis G, Brandt ME. *A neurophysiologically-based mathematical model of flash visual evoked potentials*. Biol Cybern. 1993;68(3):275-83. doi: 10.1007/BF00224863. PMID: 8452897.

36 K. C. Veluvolu, U. X. Tan, W. T. Latt, C. Y. Shee and W. T. Ang, *"Bandlimited Multiple Fourier Linear Combiner for Real-time Tremor Compensation,"* 2007 29th Annual International Conference of the IEEE Engineering in Medicine and Biology Society, Lyon, 2007, pp. 2847-2850, doi: 10.1109/IEMBS.2007.4352922.

37 Park, C.; Shin, H.; Lee, B. Blockwise *PPG Enhancement Based on Time-Variant Zero-Phase Harmonic Notch Filtering*. *Sensors* 2017, *17*, 860. https://doi.org/10.3390/s17040860

38 Lim PK, Ng SC, Lovell NH, Yu YP, Tan MP, McCombie D, Lim E, Redmond SJ. *Adaptive template matching of photoplethysmogram pulses to detect motion artefact.*

Physiol Meas. 2018 Oct 11;39(10):105005. doi: 10.1088/1361-6579/aadf1e. PMID: 30183675.

39 L. Khriji and A. M. Al-Busaidi, *"New adaptive thresholding-based ECG R-peak detection technique,"* 2018 IEEE 4th Middle East Conference on Biomedical Engineering (MECBME), Tunis, 2018, pp. 147-152, doi: 10.1109/MECBME.2018.8402423.

40 Dampney RAL. *Resetting of the Baroreflex Control of Sympathetic Vasomotor Activity during Natural Behaviors: Description and Conceptual Model of Central Mechanisms.* Front Neurosci. 2017 Aug 15;11:461. doi: 10.3389/fnins.2017.00461. PMID: 28860965; PMCID: PMC5559464.

41 De Hert, Stefan & Baerdemaeker, Luc & Maeseneer, Marianne. (2013). *What the phlebologist should know about local anesthetics*. Phlebology / Venous Forum of the Royal Society of Medicine. 29. 10.1177/0268355513501303.

42 A. Burhan, MD, *einthoven-triangle-ecg*, in Medicalopedia, November 16, 2011.

43 He, R., Wang, K., Li, Q. et al. *A novel method for the detection of R-peaks in ECG based on K-Nearest Neighbors and Particle Swarm Optimization*. EURASIP J. Adv. Signal Process. 2017, 82 (2017). https://doi.org/10.1186/s13634-017-0519-3.

44 B, Sinnapolu. *Development of a human heart rate and skin temperature monitoring system*, giri. (2015).

List of Figures

List of Tables